EVALUATING THE RELATIONSHIP BETWEEN MODIS AND AVHRR VEGETATION INDICES

JOHAN MALHERBE

School of Geosciences

University of the Witwatersrand, Johannesburg

Supervisor: Prof. H. J. Annegarn
School of Geosciences
University of Witwatersrand, Johannesburg

Co-supervisor: T Newby
ARC Institute for Soil, Climate and Water

Johannesburg, 29 March 2005

A research report submitted to the Faculty of Science,
University of the Witwatersrand, Johannesburg,
in part fulfilment of the requirements for the degree of
Master of Science.

DECLARATION

I declare that this research report is my own, unaided work. It is being submitted in partial fulfilment of the requirements for the Degree of Master of Science, in the University of the Witwatersrand, Johannesburg. It has not been submitted before for any degree or examination in another University.

Johan Malherbe 20 March 2005

ABSTRACT

This report deals with the relationship between the NDVI obtained from the NOAA AVHRR sensor and that obtained from the MODIS sensor. The relationship is quantitatively assessed for distinct polygons over various land-cover types in the northeastern Kwa-Zulu Natal Province of South Africa. Spatial and temporal variations in the relationships are addressed and discussed with reference to spectral response, sun-sensor-target geometries and atmospheric factors.

Specifically, various methods are investigated to estimate a MODIS-equivalent NDVI from the AVHRR NDVI and in so doing create the potential to develop a self-consistent NDVI between the historically available AVHRR NDVI dataset and the relatively new MODIS NDVI dataset. NOAA-16 AVHRR NDVI data and AQUA MODIS NDVI data for the two-year period from January 2002 to December 2003 are used to develop the method.

A linear relationship exists between the AVHRR and MODIS NDVI. However, spatial variations in the relationship in terms of land-cover and mean NDVI are pointed out. The potential of atmospheric corrections applied to AVHRR data through a radiative transfer atmospheric correction model to improve the relationship between the two NDVI datasets is also investigated.

The importance of geo-location accuracy of the AVHRR NDVI dataset is assessed in the light of the accuracy obtainable with the proposed method to estimate a MODIS-equivalent NDVI from the AVHRR NDVI.

A method to estimate the MODIS NDVI from the AVHRR NDVI that takes the mean AVHRR NDVI value into account, as opposed to a constant linear relationship over all the points, is proposed. Atmospheric correction is shown not to improve the accuracy of the method in a statistically significant way. The root-mean-square error of the proposed method is in the order of 0.05 NDVI units and varies between 0.5 and 2 standard deviations of the MODIS NDVI over an entire season.

ACKNOWLEDGEMENTS

I thank my supervisors Professor Harold Annegarn and Terry Newby for having guided me through this research. I also thank Philip Beukes, Dawie van Zyl and Gert de Nysschen for technical advice regarding data, software installation and programming; Brilliant Petja and Humbu Mudau for assisting in field work during site visits of the study area in 2002.

The National Department of Agriculture is acknowledged for funding the research regarding coarse resolution satellite sensors through Project 51/034. The Agricultural Research Council – Institute for Soil, Climate and Water is acknowledged for supplying the NOAA AVHRR data and allowing this research to be done during working hours. The NASA EOS Data Gateway is acknowledged for supplying MODIS imagery.

The National Land-cover information used in this report has been prepared by the National Land-cover consortium, led by the CSIR and ARC-ISCW.

This research formed part of the SAFARI 2000 Regional Science Initiative.

CONTENTS

LIST OF FIGURES

LIST OF TABLES

LIST OF ABBREVIATIONS

AOT	Aerosol optical thickness
AVHRR	Advanced Very High Resolution Radiometer
BRDF	Bi-directional Reflectance Distribution Function
CA-MVC	Constrained Angle Maximum Value Composite
DoA	Department of Agriculture
ELTOSA	Environmental Long-Term Observatories Network of Southern Africa
EON	Environmental Observatory Network
EOS	Earth Observing System
ESE	Earth Science Enterprise
HDF	Hierarchical Data Format
IQR	Inter quartile range
ISCW	Institute for Soil, Climate and Water
LDOPE	Land Data Operational Product Evaluation
LTER	Long-Term Ecological Research
MODIS	Moderate Resolution Imaging Spectroradiometer
NASA	National Aeronautics and Space Administration
NCEP	National Center for Environmental Prediction
NDVI	Normalized Difference Vegetation Index
NOAA	National Oceanic and Atmospheric Administration
RVS	Response versus scan-angle
SAC	Satellite Application Center
SAEON	South African Ecological Observatory Network
TOA	Top of atmosphere
TOMS	Total Ozone Mapping Spectrometer
VI	Vegetation Index

1. INTRODUCTION

1.1 General introduction

The purpose of this report is to investigate methods to create a continuous dataset from the Normalized Difference Vegetation Index (NDVI) product derived from the new Moderate Resolution Imaging Spectro-radiometer (MODIS) available from the Earth Observing System (EOS) with the NDVI derived from the Advanced Very High Resolution Radiometer (AVHRR) sensor on board older National Oceanic and Atmospheric Administration (NOAA) satellites. Specifically, this report deals with the relationship between NOAA-16 AVHRR NDVI and MODIS NDVI.

The NDVI is a widely used derivative of remotely sensed data utilized to monitor vegetation condition – both for natural as well as agricultural environments. The fact that it has been produced from NOAA AVHRR images continuously since the early eighties, an application not envisaged during the development of the sensor, makes the NOAA AVHRR NDVI dataset important for environmental monitoring. Furthermore, the revisit period for the satellite facilitates the acquisition of cloud-free imagery on timescales of a few days over most of the Earth, making the AVHRR NDVI a valuable tool for near real-time and long-term change detection on a global scale. In contrast to Landsat MSS imagery that was originally used quite widely in vegetation studies, the frequent coverage of any area as well as the low cost of the NOAA AVHRR imagery makes it, especially for large area vegetation monitoring, the sensor of choice.

The reason for evaluating the compatibility of the MODIS NDVI with the AVHRR NDVI is that currently a NOAA AVHRR satellite imagery dataset, spanning a period of 19 years, is being used at the Institute for Soil, Climate and Water (ISCW) for vegetation condition monitoring on a national scale. New data in the form of MODIS imagery have become available since 2000. The Department of Agriculture (DoA) has bought a receiver for MODIS data that are available for archiving and research at the ISCW. Recently, since 2004, problems with the NOAA-16 sensor have served as further motivation to start using MODIS imagery for operational monitoring, as well as for archiving in terms of being a continuation of the NOAA AVHRR NDVI dataset.

The NDVI archive at the ISCW has been derived from AVHRR data from NOAA satellites passing during the afternoon. NOAA-17, the AVHRR platform currently in use, passes over in the morning. In order to reduce the effect of a change in illumination angle, especially in mountainous areas, it has been decided that the MODIS NDVI from the AQUA platform, which also passes in the afternoon, would be a preferable continuation of the NDVI dataset from 2003 onwards. Furthermore, the influence of atmospheric phenomena has been noted in the historical AVHRR NDVI archive at the ISCW and needs to be attended to.

However, when the MODIS sensor was developed, it was intended to serve as a sensor that should be used for natural resource monitoring. The AVHRR sensor was developed for use in the field of meteorology. The difference in focus of the sensors lead to differences in terms of width and position of the channels used to derive the NDVI. One consequence is a difference in the NDVI values derived from these two sensors. It is thus important to find some way of establishing compatibility and hence continuity in the NDVI products derived between the two sensors.

The South African Ecological Observatory Network (SAEON, 2005) is the national Long-Term Ecological Research (LTER, 2005) network of observational sites that document, analyse and disseminate long-term (decades) ecological and socio-economical data. The NDVI is one of the parameters archived by EON sites while the timescale for data collected at EON sites spans several years to decades and even centuries (Henschel *et al.*, 2003). Having a continuous time series of NDVI data available since 1985 and continuing past the existence of the NOAA AVHRR program will benefit SAEON to establish natural variability, trends and extremes in vegetation activity.

Long-term monitoring of the environment is important for several reasons, including the understanding of difficulties facing resource-poor rural communities. The northeastern part of KwaZulu-Natal has been identified as a rural area with poor socio-economical conditions and environmental degradation, which have prompted the authorities to identify this area as an Integrated Sustainable Rural Development Strategy (ISRDS) node (ISRDS/1, 2000). This strategy is specifically aimed at targeting the rural poor and the importance of agriculture as a key sector of the rural economy is highlighted by the launch

of initiatives, like land-care programs and programs to enhance access to agricultural support services and markets.

The specific ISRDS Node in the north-eastern KwaZulu-Natal is referred to as Node 4 or the Umkhanyakude node. The area is important also from a conservation viewpoint, with the Hluhluwe-Umfolozi game reserve as well as the greater St. Lucia Wetland Park, an official World Heritage site, situated in this node. In the light of poverty, land degradation rate as well as natural resources and biodiversity, this node has been identified by the Department of Agriculture as a priority area for projects (Strohmenger *et al.*, 2004).

Various remote sensing projects of the ISCW dealing with soil erosion, bush encroachment and alien vegetation mapping, have concentrated their activities in this node. These include an audit on the conservation status of natural resources in this node (Strohmenger *et al.*, 2004). The node is characterized by limited infrastructure, which renders large areas problematic for obtaining surface observations. Thus remotely sensed imagery can play an important role for long-term environmental monitoring. For these reasons, the Umkhanyakude node has been chosen to be the study region for comparison of AVHRR and MODIS NDVI products.

Land-cover over the Umkhanyakude node ranges from evergreen forests with high NDVI values to savanna and resource poor agriculture with low NDVI values. The study region is characterized by a humid climate, which renders satellite images obtained over the area particularly vulnerable to atmospheric influences. If a successful method to create a self-consistent dataset from the AVHRR and MODIS NDVI can be established over this area with its challenging (in terms of remote sensing data) atmospheric conditions and diverse vegetation cover, it will serve as an indication that this method could have a more general validity and be applicable over much of southern Africa.

The study period is January 2002 to December 2003, during which both NOAA-16 AVHRR and AQUA MODIS images were available. A period of this length presents the opportunity to work with summer and winter imagery.

Image analysis, GIS and statistical software will be used to analyze image bands in visible red and near infrared wavelengths, derived atmospheric data as well as ancillary data pertaining to satellite and solar geometry. These datasets are used to develop the

normalized difference vegetation indices, and to explain or compensate for atmospheric, view and solar angle phenomena influencing the derivation of this specific index.

Studying the Earth from space has evolved into a worldwide day-to-day application. In view of continuous application of such data, the use of current technologies in conjunction with earlier datasets can attribute the dimension of historical relevance towards modern data.

1.2 Hypotheses

Main hypothesis:
It is possible, by using an easily calculated point-specific relationship between AVHRR and MODIS NDVI values, to estimate from AVHRR a MODIS-equivalent NDVI.

In order to proof the above hypothesis, the following sub- hypotheses are set out:

Sub-hypothesis 1:
A linear relationship exists between the seasonally averaged AVHRR NDVI at a site and the seasonally averaged MODIS NDVI at the site.

Sub-hypothesis 2:
All analysis must be constrained to within certain view angles to compensate for some of the effects of BRDF.

Sub-hypothesis 3:
Linear relationships for different land-cover types differ significantly.

Sub-hypothesis 4:
A mean-AVHRR-NDVI-related site-specific linear model between the AVHRR- and MODIS NDVI will yield more consistent results over a wider range of land-cover types than using a single linear model for the relationship over all sites.

Sub-hypothesis 5:
Applying a site-specific mean-AVHRR-NDVI-related linear model to estimate a MODIS-equivalent NDVI yields statistically similar results as applying atmospheric correction firstly and then a site-specific mean-AVHRR-NDVI-related linear model.

1.3 Objectives

The objectives of this report can be set out as follows:

- To perform a simple time-series comparison of AVHRR derived NDVI with a MODIS derived NDVI during the study period.
- To establish the spatial variability of the relation between AVHRR NDVI and the MODIS NDVI
- To apply atmospheric correction to AVHRR images using total atmospheric water vapor and atmospheric optical depth for aerosol as well as total ozone and satellite – sun geometry as the variable inputs to such a model.
- To evaluate the accuracy of using a constant linear model, a linear model related to the long-term AVHRR NDVI at a point and a method that combines atmospheric correction of AVHRR data with a linear model related to the long-term NDVI at the point, to estimate an NDVI value that approximates the MODIS NDVI at the point.
- To evaluate the effect of miss-registration of AVHRR imagery at the ISCW in terms of significance of influence on the derived NDVI values.
- To present the best model for the continuous data set based on the above evaluations.

2. VEGETATION INDICES FROM SATELLITE IMAGERY

2.1 Normalized Difference Vegetation Index.

Vegetation indices (VI's) are measures of vegetation parameters. They give higher values for active and dense vegetation, while stressed and sparse vegetation result in lower values. It can be derived from remotely sensed data, like satellite data. Vegetation indices must have a near linear response to plant biophysical parameters in order to be useful over the widest range of global conditions (Huete *et al.,* 1994) so that the VI values should give meaningful values for desert as well as dense forest areas, without being saturated at either end.

While vegetation reflects strongly in the near-infrared part of the electromagnetic spectrum and absorbs in the visible red part of the spectrum, reflection from bare soil for these two areas of the spectrum is almost equal. This property renders the visible red and near infrared parts of the electro-magnetic spectrum popular wavebands for use in vegetation indices. The Normalized Difference Vegetation Index (NDVI) is a ratio index that employs the difference in the reflectance between these two parts of the electro-magnetic spectrum to indicate the activity of vegetation:

$$NDVI = (NIR - RED) / (NIR + RED)$$

While the upper bound of the NDVI approaches 1, the lower bound of the NDVI approaches zero.

The NDVI value is determined by the absorption of the red wavelengths through chlorophyll (proportional to leaf chlorophyll density) and by the reflectance in the near-infrared wavelengths that is proportional to green leaf density (Tucker *et al.*, 1985). It therefore is related to biophysical vegetation variables such as fraction of absorbed photosynthetically active radiation (Goward and Humerich, 1992) and Leaf Area Index (Hatfield *et al.,* 1985). It is a very widely used index for monitoring vegetation globally and has been used through NOAA AVHRR data as input to monitoring of drought (Ramesh *et. al.*, 2003), estimation of global net primary production (Wessels *et al.*, 2004, Awaya *et al.*, 2004) and crop-growth modeling and yield prediction (Dabrowska-Zielinska

et al., 2002, Jiang *et al.*, 2004, Reynolds *et al.*, 2000, Kalubarme *et al.*, 2003, Maselli *et al.*, 2000).

Contamination of the NDVI occurs as a result of background color (Huete, 1988) as well as through the influence of atmospheric constituents like water vapor (Justice et. al., 1991) and view-target-sun geometries (Holben, 1986). In some studies it has been shown that the NDVI does not respond to variations in Leaf Area Index in densely forested areas, indicating the tendency to saturate with high biomass and not being linear over these regions (Huete and Justice, 1996).

2.2 Characteristics of NOAA AVHRR

The National Oceanic and Atmospheric Administration (NOAA) satellite series has been developed for meteorological purposes. Sensors on meteorological satellites generally have a coarser spatial and spectral resolution than land oriented satellite systems (Lillesand and Kiefer, 2000). The NOAA satellites are sun-synchronous polar orbiting platforms with an altitude of 850 km. The view angle of the AVHRR is 55.4°, with a resultant swath width of 2 400 km. A NOAA satellite has an orbit repeat period of 4 to 5 days (Cracknell, 1997; Lillesand and Kiefer, 2000).

Advanced Very High Resolution Radiometer (AVHRR) sensors have been flown on a series of NOAA satellite platforms, from NOAA-6 to the current NOAA-17 and future missions until the launch of the NPOESS platform by 2009, which will carry the successor to the AVHRR. While the NOAA-6, -8,-10,-12,-15,-16 and –17 satellites have day-time overpasses, the NOAA-7,-9,-11 and -14 have night time overpasses. The AVHRR sensors flown on the earlier NOAA satellites had four or five channels (AVHRR-2 and AVHRR-3), but since NOAA-15, the satellites carry a 6-channel AVHRR sensor. However, all these AVHRR sensors had both a red and a near-infrared channel. The red and near infrared channels are used to calculate the normalized difference vegetation index (NDVI).

Apart from the two visible channels in the AVHRR instruments (red: 0.58 – 0.68 μm and near-infrared: 0.725 – 1.10 μm) remaining channels are in the window regions of the mid infrared and thermal infrared region of the spectrum (3.55 – 3.93 μm, 10.3 – 11.5 μm, 11.5 – 12.5 μm).

2.3 Characteristics of MODIS.

The Moderate Resolution Imaging Spectroradiometer was launched in December 1999 on the TERRA platform (TERRA, 2004). TERRA is the name, meaning Earth in Latin, of the flagship satellite of the Earth Observing System (EOS). The EOS, composed partially by a series of satellites, is intended to improve the understanding of the Earth as an integrated system. EOS is the centerpiece of NASA's (National Aeronautics and Space Administration) Earth Science Enterprise (ESE), dedicated to understanding the total Earth system and the effects of natural and human-induced changes on the global environment (NASA, 2004). The MODIS sensor is flown on both the TERRA and AQUA (the second satellite of EOS) missions and it is also envisaged to be on their follow-up missions. Its design is rooted in various heritage instruments, like the AVHRR (Lillesand and Kiefer, 2000). On the TERRA mission alone, it provides two-day repeat coverage of the Earth, however the repeat time for exact overpass for MODIS is sixteen days. This means that subsequent passes produce different views of the same area on Earth. Figure 2.1 shows the position of the MODIS TERRA swath for four consecutive days. The sensor passes at 10:30 am on TERRA and a second MODIS on the AQUA platform (launched in May 2002) provides afternoon and night observations at 2.30 pm and 2.30 am.

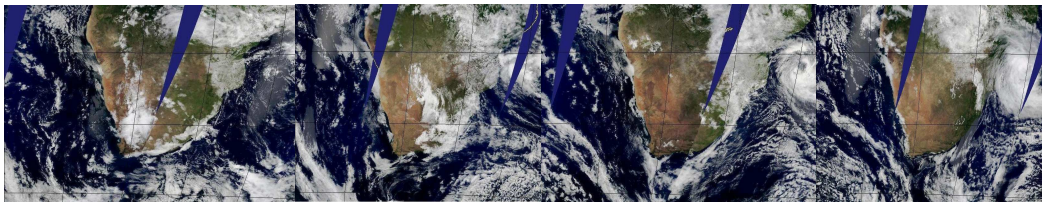

Figure 2.1 MODIS swaths for four consecutive days over southern African region. (Modified from: MODLAND Browse, 2005).

The total field of view of MODIS is 55°, providing a swath width of 2 330 km. MODIS has the highest number of spectral bands of any global coverage moderate resolution imager. It collects data in 36 carefully chosen spectral bands (Table A1, Appendix 1) with 12-bit radiometric sensitivity. The bands were chosen to lie within atmospheric window areas (Figure 2.2 and 2.3). The MODIS red and near-infrared bands respectively have much narrower bandwidths (0.620 to 0.670 μm and 0.841 to 0.876 μm) than their

counterparts on the AVHRR (0.580-0.680 µm and 0.725 to 1.080 µm) (Vermote and Vermeulen, 1999).

The availability of 7 bands in the 0.41 – 2.1µm spectral interval enables the derivation of aerosol loading for improved atmospheric correction. The 250-m bands (Channel 1 and 2 – red and near-infrared) are used to develop cloud masks that are more accurate than possible with 1km resolution bands. A mid-infrared channel (Band 26 – Table A1) is used to detect thin cirrus, making it possible to correct for these stratospheric influences for the first time, and another mid-infrared channel (Channel 20 – Table A1) aids in algorithms to derive aerosol optical thickness (Vermote and Vermeulen, 1999) used during atmospheric correction of the imagery.

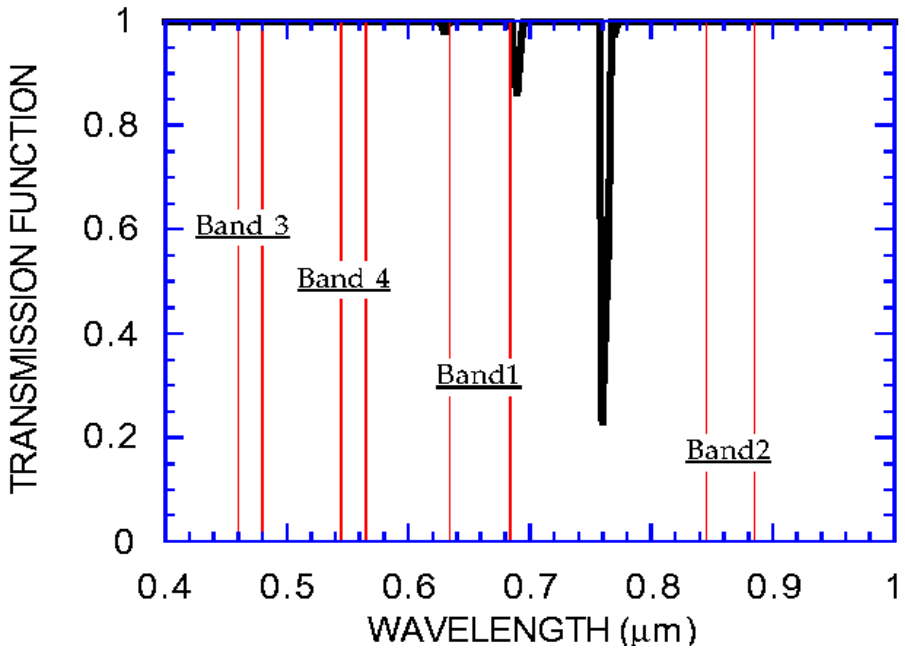

Figure 2.2 Gaseous absorption by ozone for MODIS channels over the indicated wavelengths. (Vermote and Vermeulen, 1999).

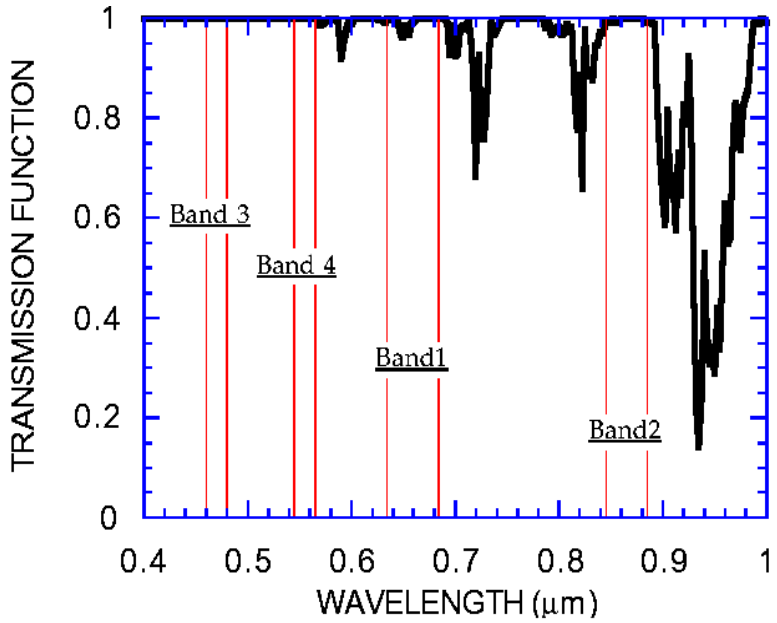

Figure 2.3 Gaseous absorption by water vapor for MODIS channels over the indicated wavelengths (Vermote and Vermeulen, 1999).

An important prerequisite for remote sensing data to be used operationally to detect change over time is that the pixels for a specific location for different times should overlay each other. Satellite data production systems operationally register different orbits of data by geometric correction of each orbit into a common Earth-based coordinate system. Getting proper geo-location is more difficult as the resolution of an image becomes coarser. The TERRA satellite has on-board exterior orientation (position and altitude) measurement systems designed to enable geo-location of MODIS data to approximately 150-m, but a global network of points (extracted within 24 km square chips from 121 precision geo-located terrain corrected Landsat 4 and 5 scenes) has been used to determine biases and trends in the sensor orientation. The biases have been removed by updating models of spacecraft and sensor orientation in the MODIS geo-location software, improving the geo-location to approximately 50 m. This accuracy is sufficient to allow the creation and analysis of science products by users without first incurring the delays and costs associated with improving geo-location accuracy (Wolfe *et al.*, 2002).

The on-orbit performance of the sensor has been satisfactory. The signal-to-noise ratios for the reflected solar bands, as well as the noise-equivalent radiance for the thermal infrared

bands, are meeting pre-launch expectations. Some artifacts detected during the operation of the sensor include (Guenther *et al.*, 2002):

- Incomplete knowledge about the response versus scan angle (RVS) for the TERRA MODIS instrument – it was not determined prior to the launch and other methods, like AQUA RVS values, are used to characterize this effect.
- Reduced response is present in the visible and short wave infrared bands as the result of scan mirror and solar diffuser degradation. These problems are resolved by solar diffuser based calibration (at instrument temperature).
- A fixed pattern noise of 1 – 2 resolution units is present and is correlated to the complete rotation of the scan mirror.

Reprocessing of MODIS data has been implemented since data transfer started. As improved algorithms are developed, these improvements are implemented through reprocessing all prior images and derived products. Outputs from the first major reprocessing are referred to as "Collection 3 data". In February 2003, Collection 4 images became available. Collection 4 images are in sinusoidal projection, which causes less distortion when changing the projection of images to projections widely used by GIS specialists than the integerized sinusoidal projection that was used for the Collection 3 data. Images in sinusoidal projection can also be recognized by a larger number of commercially available image-processing software. Other improvements in the Collection 4 data include better data filtering before compositing, aerosol consideration in data filtering and better spatial consistency after compositing (features are more clearly definable) – not previously available. Some known issues remain: Compositing over persistent clouds is still problematic due to the mislabeling of cloudy pixels. There are problems with aerosols due to poor performance of the aerosol correction algorithm (TERRA Readiness Document (2004)).

Comparison of preliminary MODIS surface reflectance data with point measurement enhanced ETM imagery has indicated a less than 5% absolute error in reflectance values (Liang *et al.*, 2002).

Validation of MODIS products have been undertaken in numerous campaigns involving international collaboration, like the South African Regional Science Initiative (SAFARI 2000) (*King et al.*, 2002). A core site network for validation, representative of global biomes and land cover characteristics, has been established. Skukuza, in the Kruger

National Park, is one of the sites (Morisette *et al.,* 2002). SAFARI 2000 was a regional project investigating emissions, transformation and deposition of trace gases and aerosols over southern Africa. One of the specific aims of the SAFARI 2000 initiative was to validate and calibrate remotely sensed observations of the bio-geophysical system of the southern African subcontinent derived from NASA's Earth Observation System (EOS) TERRA satellite (Swap *et al*., 2002). This was done by implementing the NASA ER-2 aircraft flying at an altitude of 20 km and serving as a customized satellite with sensors equivalent to those on the TERRA and AQUA spacecraft.

The MODIS products represent for the first time global terrestrial products, that have been systematically atmospherically and bi-directionally corrected (corrected for differing sun and view angles) available to a very wide community of users. Products from MODIS also include the most comprehensive Quality Assessment metadata ever provided in the context of terrestrial remote sensing. Being sensed from a platform with other instruments also involved in terrestrial remote sensing, there exists great opportunities for the use of multi-sensor data for new products and for the enhancement of products (Townshend and Justice, 2002).

MODIS vegetation indices are intended to serve as an improvement on indices currently available, enabling users to identify land cover change more quickly (Huete and Justice, 1996). They have been designed to provide consistent, spatial and temporal comparisons of global vegetation conditions that can be used to monitor photosynthetic activity (Justice *et al.,* 1998). Two Vegetation Index products developed from MODIS data include the NDVI (Normalized Difference Vegetation Index) and the EVI (Enhanced Vegetation Index). While the NDVI is chlorophyll sensitive, the EVI, for which, in addition to the red and near-infrared, the blue band is also used, is more responsive to canopy type, plant physiognomy and canopy structure (Gao *et al.*, 2000) and does not saturate over high biomass as easily as the NDVI (Fensholt, 2004). The MODIS NDVI is referred to as the "continuity index" to the existing NOAA derived NDVI (Huete *et al.*, 2002) and therefore the relation between the EVI and NOAA NDVI is not investigated in this report.

Sources of noise in the MODIS Vegetation Indices (VI's) include the 5% absolute sensor calibration accuracy in bands 1 (red), 2 (near-infrared) and 3 (blue), and an error associated with a 10% band-to-band co-registration goal (±50 m) in the cross- and along-track

directions. Of concern in the compositing of the MODIS VI's are the following: Geo-location of images and accurate geometric registration, preferably to within 0.1 pixels; and uncertainties present in cloud screening, atmospheric corrections and BRDF products. Environmental sources of error and uncertainty include atmospheric variations, sun and view angle differences of different pixels and background variations. (Huete and Justice, 1996, Huete *et al.*, 2002).

2.4 Sources of differences in NDVI values for different sensors

There are numerous causes of different NDVI values derived for the same time and area from different satellite sensors. Some of these causes result in constant differences, while others result in differences that vary in time and space. The difference in spectral response of sensors to certain wavelengths due to different spectral response functions or calibration differences (Gutman, 1999), different spatial resolution, solar and satellite view geometry and atmospheric effects in the form of water vapor and aerosol absorbance and scattering are all factors influencing the derived reflectance values for each sensor, which in turn influences the values of the derived NDVI values (Holben and Fraser, 1984; Trischenko *et al.*, 2002).

2.4.1. Spectral resolution

Systematic differences in response of different sensors occur because the channels in certain spectral bands receive somewhat different components of the reflectance spectra of vegetation and soil (Gallo and Daughtry, 1987). The sensitivity of spectral reflectance to chlorophyll content varies widely in the visible range of the spectrum (Gitelson and Merzlyak, 1996). Therefore, the exact position of the red band influences the value of the NDVI. MODIS bandwidths in the red and near infrared parts of the spectrum are much narrower than the corresponding channels in the AVHRR. The red band of NOAA AVHRR ranges from 0.58-0.68 μm, while the MODIS red channel ranges from 0.62 to 0.67 μm. In the case of the near infrared channel, the AVHRR bandwidth is from 0.725 to 1.080 μm, while in the case of MODIS it spans 0.841 to 0.876 μm. The narrow bandwidth of the MODIS channels is chosen to eliminate the water absorption in the near-infrared band and to make the red band more sensitive to chlorophyll absorption. Figure 2.4 gives an indication of the difference between AVHRR and MODIS bandwidths and the amount of water vapor absorption within the bandwidths.

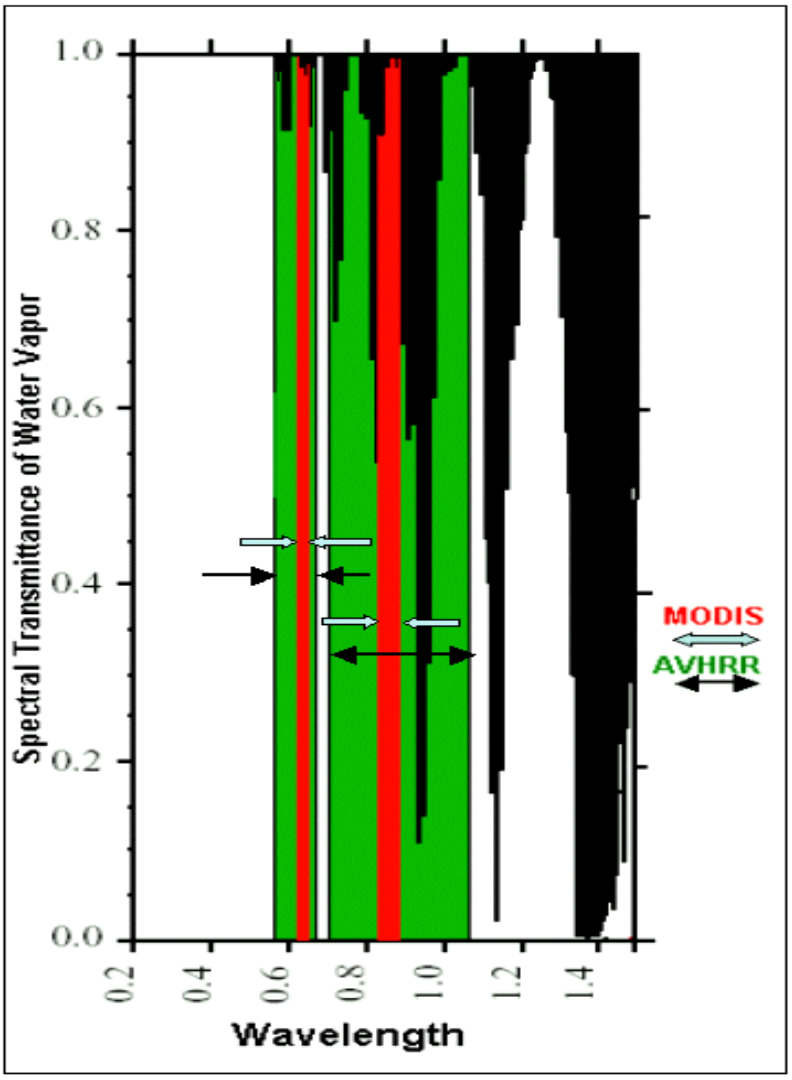

Figure 2.4 MODIS and AVHRR bandwidths for the red and near-infrared channels (Modified from Vermote *et al*., 1997c).

In a study over forested and desert areas, MODIS and AVHRR NDVI values were found to mimic each other closely, but the seasonal variability for the MODIS NDVI values were greater than for the AVHRR (Fensholt, 2004). A Study conducted in a laboratory have concluded that because the AVHRR red band is wider than the MODIS red band a combination of the MODIS red and green bands should be used to represent the AVHRR red channel in order to avoid a step in the NDVI of up to 0.05 (Gitelson and Kaufman, 1998). In another study conducted on plant matter in a laboratory, a linear relation between the NDVI values of different sensors was found (Steven et al, 2003) for agricultural

vegetation. The following model was suggested the relation between the NDVI values for MODIS and AVHRR:

NDVI (MODIS) = 0.004 + 1.103 * NDVI (AVHRR).

However, the influence of spectral response of satellite sensors to Vegetation Indices from different satellite sensors can not be compensated for by linear adjustments between sensors unless calibration, atmospheric correction and correction for the bidirectional response takes place beforehand (Coetz, 1997: Steven *et al.*, 2003). Studies conducted with spectrometers in laboratories do not take the influence of atmospheric conditions or view angle into account.

2.4.2. Atmospheric influences

Atmospheric effects limit the accurate estimation of surface shortwave reflectance (Zhao *et al.*, 2000). The effects of the atmosphere on AVHRR data mostly represent atmospheric scattering and absorbing. This can either increase or decrease the NDVI depending on the attenuation of the red and near-infrared channels (Holben, 1986).

Atmospheric water vapor influences mainly the near-infrared channel of the AVHRR (Rahman and Diedieu, 1994; Holben, 1986), while atmospheric scattering by aerosols causes the difference in reflectance between the red and the-near infrared bands to decrease, lowering the vegetation index values (Justice *et al.*, 1991). Furthermore, the atmospheric path-length, which is a function of sun-sensor-target geometry can exacerbate these influences which can be reduced by high sun angles, constrained view angles and clear atmosphere (Holben and Fraser, 1984). Optically thick Clouds Suppress the NDVI value through reflecting equally in the red and near-infrared regions of the electromagnetic spectrum (Moody and Strahler, 1994). Furthermore, cloud shadow also causes a decrease in the NDVI (Simpson and Stitt, 1998).

The Maximum Value Composite method was designed to reduce the effect of cloud, atmosphere and variable illumination on the NDVI. However, tradeoffs are made between compositng period and elimination of atmospheric effects (Holben, 1986). It has been noted from the dataset of the ISCW that 10-day composite NDVI values are lower during certain wet seasons when atmospheric water vapor concentration and cloud cover were higher than normal.

Between the MODIS and AVHRR NDVIs the influence of the atmosphere, as described above, has also been noted. Over humid areas, discrepancies between the sensor NDVIs have been found to be larger than over drier areas. A major cause of the differences has been established to be the influence of water vapor content in the atmosphere, which strongly affected the AVHRR-NIR band and caused NDVI values to decrease, especially during the more humid, wetter part of the season (Huete *et al.*, 2002).

For common ranges of precipitable water in the atmosphere, the NDVI can be lowered by 0.02 units (Holben, 1986) and for some recorded precipitable water content values even up to 0.08 units (Goward *et al.*, 1991, Justice *et al.*, 1991). Absorption by other atmospheric constituents like ozone, oxygen and other trace gasses can also suppress NDVI values (Holben, 1986). Oxygen lowers the NDVI by less than 1% (0.01 units) under normal atmospheric conditions as a result of suppressing the near-infrared channel response. The attenuation of the NDVI by ozone is also small and the concentrations thereof well known. Aerosols also, by increasing optical depth of the atmosphere in times of heavy aerosol loading, can suppress the NDVI by as much as 0.2 units (around 20%) (Huete and Justice, 1996).

Methods used to correct for atmospheric effects include: using bare sand pixels as a reference over arid areas (Chi, 2003), pixels with very dense vegetation for more vegetated areas (Kaufman and Sendra, 1988) and using deep water pixels to derive aerosol scattering in the red channel (Salama and Monbaliu, 2004). However, the main method used to correct for the influence of the atmosphere is through the application of atmospheric radiative transfer models. These models are much more data intensive in terms of atmospheric properties such as vertical profiles of water vapor, temperature and aerosols than the other methods referred to. Data regarding these properties can be difficult to obtain (Chi, 2003) or could be available on a very coarse resolution (Wessels *et al.*, 2004). Simplifications of these models in the form of semi-empirical formulas describing radiative transfer for specific sensors have been developed (Rahman and Diedieu, 1994).

A widely used radiative transfer atmospheric correction model is the “6S” code (Vermote *et al.*, 1997a). This code is physically based and can handle a wide range of satellite sensors and optional wavelengths (Zhao *et al.*, 2000). It has been used to verify the MODIS operational atmospheric correction algorithm (Vermote *et al.*, 1997b) and has also

been used in studies incorporating the atmospheric correction of AVHRR data (Hanan *et al.*, 1995, Hu *et al.*, 2000). Input data to the model include cloudless reflectance, geometrical conditions, temperature and water vapor profiles, aerosol type and concentration (Vermote *et al.*, 1997 c). Two limitations of the 6S code are the difficulty in acquiring atmospheric data as well as computation time.

2.4.3. Effect of Bi-Directional Reflectance Distribution Function (BRDF)

Spectral radiance measured in the shortwave visible and near infrared parts of the electromagnetic spectrum by wide swath space-borne remote sensing instruments such as the AVHRR retain a dependence on the sun-target-sensor geometry of the observation (Wu *et al.*, 1995) as the result of the fact that many land cover classes do not behave as Lambertian surfaces. Bidirectional Reflectance Distribution (BRD) effects in 1.1 km resolution AVHRR data vary with spectral band, land cover type and satellite zenith and azimuth angles (Cihlar *et al.*, 1994). Furthermore, apart from being land-cover specific, the BRD has also been shown to vary significantly with the NDVI (Wu *et al.*, 1995). The wide range of angles from which the AVHRR sensor records data also is a major cause of problems in this regard.

BRDF effects have been observed in single day as well as composite AVHRR data and corrected with the use of midday pass data for six land-cover types over the Boreal ecosystem (Cihlar *et al.*, 1994, Li *et al.*, 1996) It has been shown that corrections should be applied to the red and near infrared channels of different land-cover types separately The BRD effect was also observed to be one of the major causes of noise in the MODIS vegetation index composite images (Huete *et al.*, 2002).

In order to estimate the BRDF effect from remotely sensed data, surface directional behavior must be described by models that can be inverted by sufficient multidirectional data (Chopping, 2001). Kernel BRDF models are semi-empirical models that estimate reflectance by using linear combinations of component reflectance and kernels. These kernels are functions that depend on sun and view angles. The physical bases for the kernels include geometric as well as volume (path length and scatter) factors (Jupp, 2000). These models are inverted with multi-directional data.

The semi-empirical Roujaen BRDF model is one such kernel model developed especially for available remote sensing data from polar orbiting satellites in use today (Roujean *et al.*,

1992). It has been shown to work with reasonable accuracy over semi-arid grassland areas when data from both morning and afternoon AVHRR sensor passes are used (Chopping, 2001). It can be implemented in the 6S atmospheric correction code for homogeneous targets when the parameters for the model are provided (Vermote *et al.*, 1997c).

2.4.4. Compositing method

For the sake of obtaining spatially complete, cloud-free imagery over the Earth, composites utilizing data from more than one overpass are made of Vegetation Index products. In order to attain cloud-free pixels close to nadir, especially over areas that experience frequent cloud cover, the compositing period should be long (Huete and Justice, 1996).

One such compositing method is the Maximum Value Composite (MVC) method. This method selects on a per pixel basis the highest NDVI value for the period. The MVC is primarily formulated to reduce residual cloud effects not accounted for in the cloud masking procedure, as well as atmospheric sources of contamination that lowers the NDVI Through using the pixel with the maximum TOA reflectance and hence assumed minimum atmospheric interference, these influences are reduced (Holben, 1986). However, it does not eliminate these problems. Its major shortcoming is that bi-directional influences of the surface are not adequately accounted for.

As the result of the spectral dependence of the bi-directional reflectance distribution function (BRDF) (where the near-infrared response is more anisotropic than the red), the method favors the forward scattering direction of off-nadir pixels (where more vegetation and less background is effectively viewed by the sensor). Cloud contamination is still a problem since off-nadir, contaminated pixels can still give higher NDVI values than nadir, clear pixels. Selection of off-nadir pixels causes higher NDVI values to be selected than is actually the case at a specific location on Earth and can even contribute to the saturation problem experienced with non-linear indices like the NDVI (Huete and Justice, 1996). One precaution that is taken for this effect is to make use of only data that was sensed within a certain view angle − the Constrained Angle MVC (CA−MVC).

Miss-registration of individual images can also influence the maximum value composite technique negatively in terms of choosing pixels with higher NDVI values shifted to a specific point instead of the lower pixel value that should overlay that point (Holben, 1986).

The MODIS standard NDVI product is based on images spanning periods of 16 days. This is partly based on attaining a symmetric view-angle-distribution over the 16-day MODIS repeat-cycle (Huete and Justice, 1996). The compositing methodology for MODIS data should rely on the cloud mask, atmospheric correction information, view- zenith angle, relative azimuth angle and on surface BRDF normalization where more than five cloudless scenes are available in a 16-day compositing period. The algorithm utilizes the information in the MODIS surface reflectance product quality check data to preprocess Bands 1 and 2. In this way it is assured that land pixels with clouds, shadows and bad data integrity will be excluded from the compositing process.

Three algorithms can be used to make composites of MODIS NDVI data (Huete and Justice, 1996; Huete *et al.*, 2002):

- *The bi-directional reflectance distribution function composite.* If five or more pixels pass the initial screening for a specific location, this method is used. The method relies heavily on the correctness of the cloud mask. A nadir equivalent radiometric value is interpolated from five measurements and one contaminated pixel will compromise the final computed nadir value. Vegetation is most active when most cloud cover occurs, and this causes this module to be largely constrained to the part of the season where the least vegetation activity occurs or dry periods or areas with low vegetation activity, like deserts.
- *The constrained angle maximum value composite*. This method is used when less than five pixels pass the initial screening. The two pixels with the highest values are selected and from them the one with the smallest view angle is selected. If only one good observation is available, the data from this pixel is used.
- *The maximum value composite* technique is used when no pixel passes the initial data screening.

It has been found that residual cloud and atmospheric effects still linger in the composite MODIS data. The constrained angle maximum value compositing technique is the main method being used to composite MODIS vegetation indices as the result of the need of five clear views in a compositing period for the BRDF method. The view angle for composite pixels has been constrained to about 30° off nadir (Huete *et al*., 2002).

It is intended to shorten the period for the vegetation index composites also to 8 days with the addition of the Aqua platform. However, such data are yet to be made available.

While the MODIS compositing method only utilizes data within 30 degrees, the method used for compositing AVHRR NDVI data implemented at the ISCW constrains the angle only to 45 degrees. This MVC method and a cloud mask are used to make AVHRR NDVI composites. At the ISCW any length can be chosen for a compositing period because the data resides in raw format and composites are made in-house. Methods will be described in the following chapter.

3. IMAGE PREPARATION AND EXTRACTION OF NDVIs

3.1 Area of Interest

The Umkhanyakude node is situated on the northeastern corner of Kwa-Zulu Natal (Figure 3.1). It borders on the Indian Ocean in the east where natural forests and forest plantations are found. Sugar is also cultivated over the southeastern areas (Figure 3.2). Further inland the land-cover ranges between savanna and grassland, with some areas cultivated (subsistence dry-land agriculture and commercial dry-land agriculture) while forests prevail among mountainous areas. The St. Lucia estuary in the southeast is surrounded by a wetland that forms part of the greater St. Lucia Wetland Park. The lack of built-up residential or commercial areas is an indication of the rural nature of the node.

Seventeen circular polygons with radii of 2 km were used to extract data from AVHRR and MODIS imagery. The national land cover map for South Africa (Fairbanks *et al.*, 2000) and photographs taken on a field trip in specific biomes were used to identify areas within the region where representative data could be obtained. The polygons are indicated together with the land-cover of the node in figure 3.2.

The extraction of data-per- polygon and not data-per-pixel was done to attenuate the errors due to possible minor miss-registration between images. The polygons were chosen over areas representative of the range of vegetation types identified and most of them had been visited in 2002.

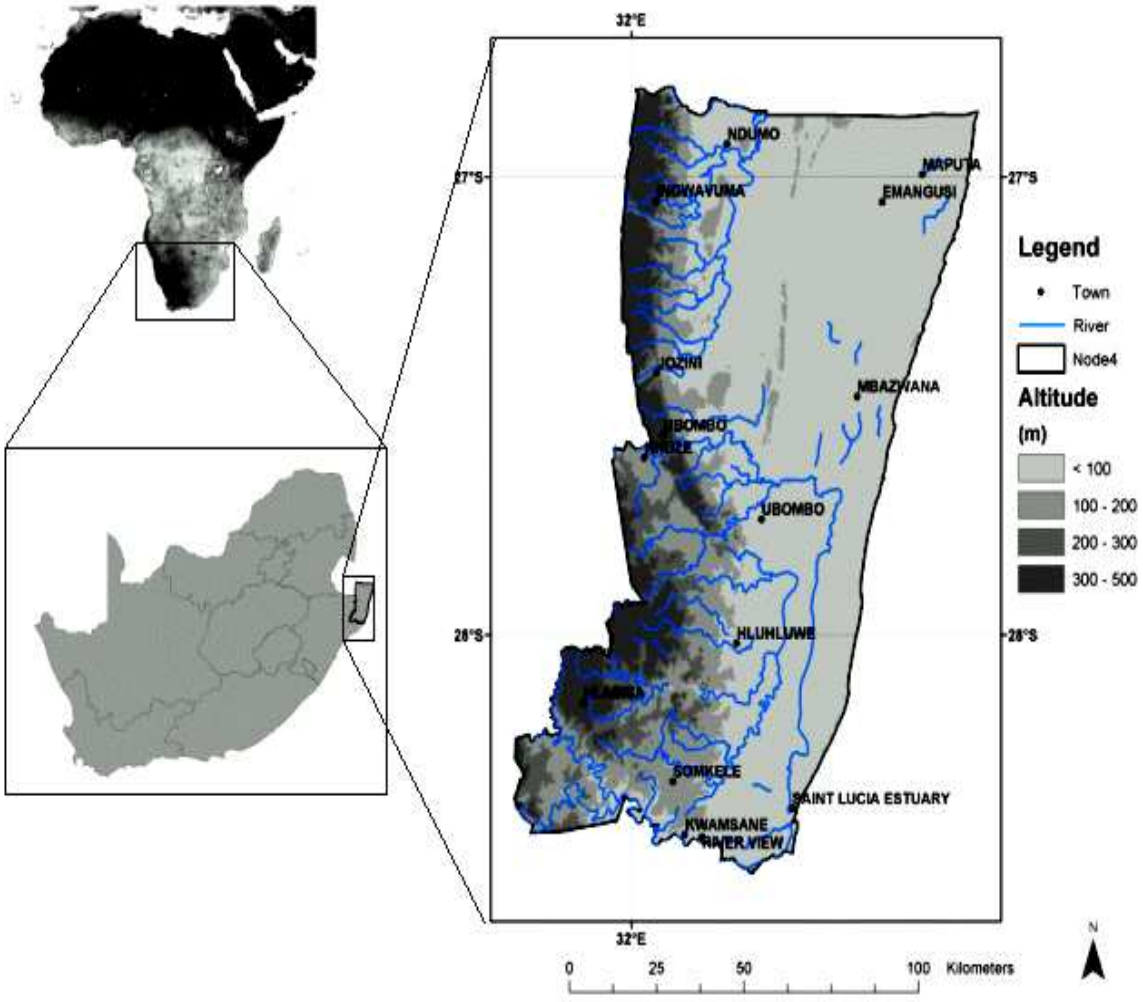

Figure 3.1 The Umkhanyakude node.

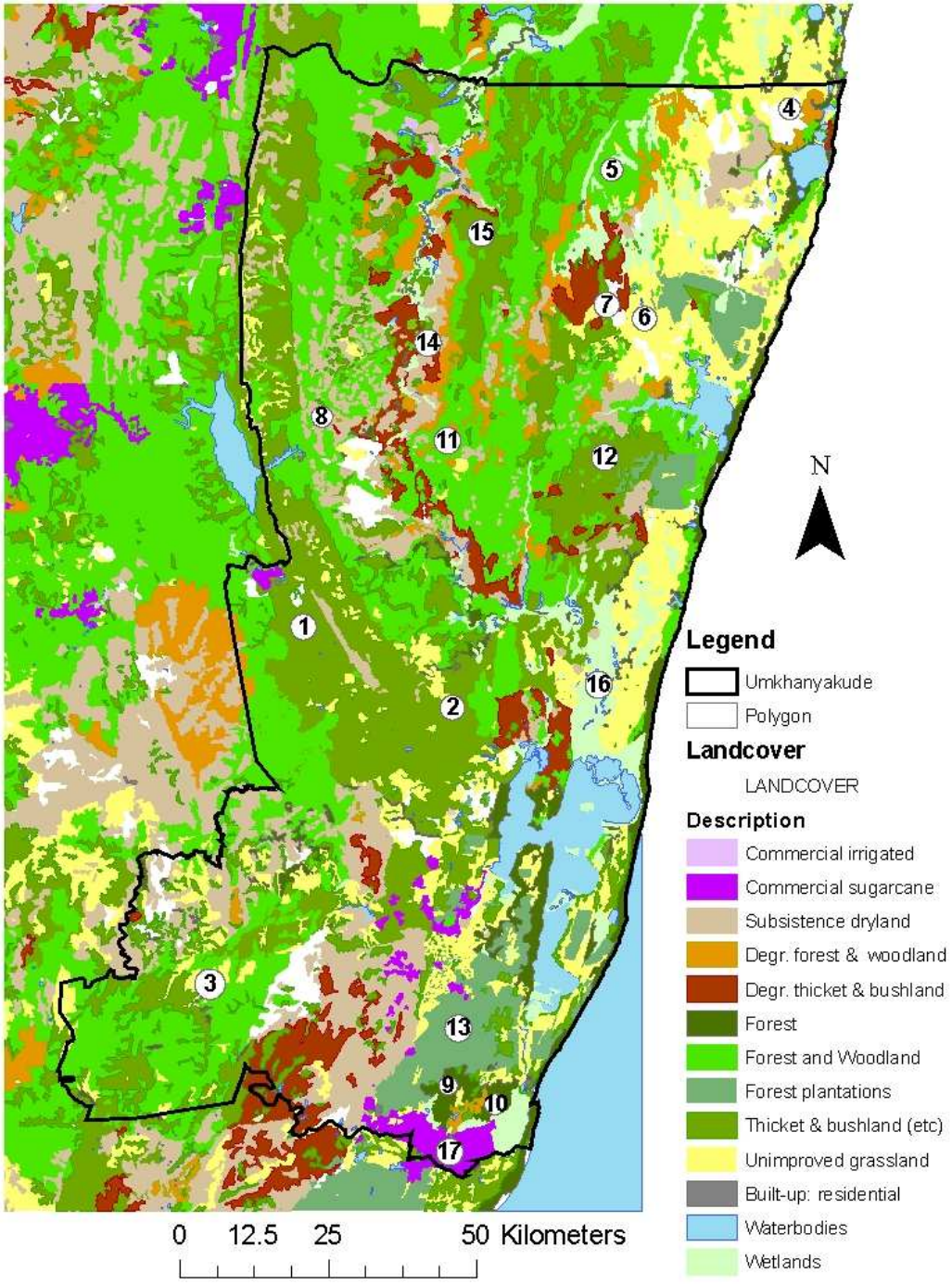

Figure 3.2 Land-cover types of the Umkhanyakude node and the 17 polygons for which NDVI composite and daily MODIS and AVHRR red and near-infrared channel values were extracted.

3.2 NOAA AVHRR data products

NOAA AVHRR data are received at the Satellite Application Center (SAC) at Hartbeeshoek, from where it is downloaded via FTP to the ISCW in Pretoria and archived in a server at the National Department of Agriculture. One of the major advantages of the AVHRR dataset is that it hosts data since February 1985 and therefore provides the opportunity of working with current as well as historical data in environmental monitoring programs. The geographical extent of the AVHRR data downloaded and stored by the ISCW includes the entire Africa south of about 5° southern latitude (Figure 3.3).

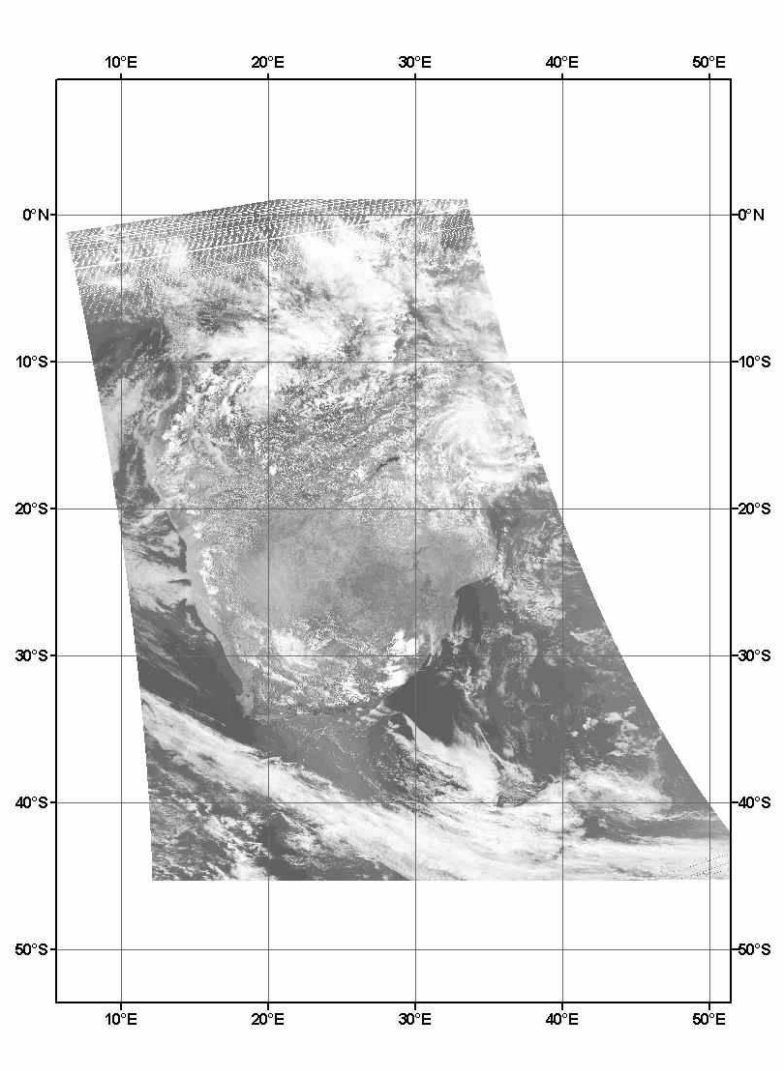

Figure 3.3 A NOAA AVHRR scene archived at the ISCW.

Images are available at a 1.1 km resolution (Level 1B Local Area Coverage). A total of 9 channels are received per scene. These include the two visible channels, three thermal channels as well as four channels with the Sun- and Sensor azimuth- and zenith angle information. The size of an entire level1B scene is 80 MB. At the ISCW, AVHRR data are processed with software called CHIPS (Hansen, 1999), developed especially for AVHRR. Processing results in a separate image in CHIPS .img format for each channel. From CHIPS the various channels can be exported in an 8-bit GeoTiff format or as 32 bit data in an ASCII file format. The size of the 8-bit GeoTiff file is 17 MB while the size of a 32-bit ASCII file is 160 MB per channel.

NOAA AVHRR instruments are calibrated before launch by the determination of the spectral response function of each spectral channel as well as the radiometric calibration of all five channels. There is also in flight calibration of the thermal infrared channels while post launch calibration studies have been done on the two visible channels (Tahnk and Coakley, 2001; *Heidinger et al.*, 2003, Rao and Chen 1995, 1996).

Calibration of the imagery for all the channels are done at the Institute for Soil, Climate and Water by combining the raw images with data in the header files of the images. The header file contains the calibration coefficients as well as the calibration table. This results in a top-of-the-atmosphere-reflectance image for the visible channels. Sensor degradation of the visible channels is also addressed through the method that takes the amount of days since the launch of a specific instrument into account (RAO and Chen, 1995, 1996). Another way of compensating for sensor degradation in the visible channels of the AVHRR data at the ISCW is to plot the visible channel (red and near-infrared) responses for a specific area where no change is expected (an area in the Namib Desert) and to determine the slope of the graph over the long-term for each AVHRR sensor.

Geo-location of the AVHRR products at the ARC ISCW is done automatically. Two Line Elements (TLE's), which carries information on the position of the satellite relative to area covered, are downloaded from the Internet (Celestrak, 2005). These are used in conjunction with 300 base images containing control points to which cloudless areas on a scene are fitted. Geo-location can be negatively affected when a large amount of the control points are covered by clouds. The accuracy of the geo-location procedure varies

between 1 and 2 pixels but when large areas are covered by cloud, the accuracy can be as low as 3 pixels.

All the NOAA AVHRR data used for this report were taken from the NOAA archive at the ISCW. Data used included daily NDVI images and daily visible red and near-infrared reflectance (Channel 1 and 2) as well as solar zenith-, solar azimuth-, view zenith- and view azimuth- angle channels.

NDVI images are derived automatically from AVHRR data with an algorithm developed at the ISCW utilizing CHIPS. The NDVI is derived from channels 1 (0.58 – 0.68 μm) and 2 (0.73 – 1.1 μm) of the AVHRR. Cloud detection is handled through a procedure that combines the Top of Atmosphere (TOA) reflectance from channel 1, the brightness temperature from channel 4 (10.30 – 11.30 μm) and the difference in brightness temperature between channels 4 and 5 (11.50 – 12.50 μm) (Agbu and James, 1994).

After production, NDVI values are scaled to between 1 and 255, a data range that can be stored as an 8-bit GeoTIFF image. Operationally, routine composites are made on a ten-day basis using the Constrained Angle Maximum Value Compositing (CA-MVC) technique that was developed to diminish the influence of atmospheric effects. No other atmospheric corrections are applied.

MODIS NDVI products are available from the EOS Data Gateway only as 16-day composites, while NOAA AVHRR data are available daily, and composites of any length can be made. For this report, to allow direct comparisons between AVHRR and MODIS NDVI images, 16-day AVHRR NDVI composites were made. The resulting CHIPS 16-day composite images were processed into GeoTiff format with a Plate Carree (Geographic/Simple Cylindrical) projection.

Apart from NDVI data for the 16-day composites, daily Level 1b AVHRR images were also converted into the same format as the 16-day composites, for selected days when both NOAA-16 and AQUA passed over the area of interest with little or no cloud cover. AVHRR channel 1 and channel 2 images were processed to 32-bit ASCII data to allow for a finer radiometric resolution than what can be stored in 8-bit GeoTiff imagery. The daily AVHRR NDVI images and the Quick Browse website for MODIS (Global Browse Website, 2005) were examined to establish whether cloud cover was absent or sparse enough to justify the effort of obtaining imagery for both sensors on a given day.

3.3 MODIS data products

All Earth Observing System (EOS) data products are stored using an enhanced hierarchical data format (HDF-EOS) that allows data access via an HDF toolkit. In the case of MODIS data, various tools have been made available to convert the data into a format recognizable by remote sensing and GIS software by the Land Distributed Active Archive Center (LDAAC). The Earth Observing Data System in South Dakota is responsible for the archive, production and distribution of MODIS land products. Over 10,000 files, with a total data volume in excess of 390 GB, are produced in the processing of land products only for TERRA MODIS daily (Justice *et al.*, 2002).

The MODIS data are downloadable via File Transfer Protocol (FTP) from the Earth Observing System Data Gateway (EOS Data Gateway, 2005). It can also be shipped on CD or DVD. FTP and shipping both are free of charge. To assist in the choice of dates for specific data, coarse spatial resolution representations (5 km) of MODIS land products have been developed on the Global Browse website for synoptic evaluation at reduced data volume (MODLAND Browse, 2005).

MODIS images from the Earth Observing System are available in tiles numbered both longitudinal and latitudinal across the globe. South Africa is covered by 4 tiles (Figure 3.4). For certain days, the swath of the sensor can go entirely through a tile, on other days the swath can go only through the peripheries of the tile.

Daily surface reflectance imagery is one of the products available from the EOS Data Gateway. The MODIS daily surface reflectance product is labeled: MOD09. A MOD09 tile consists of:

- Channel 1 to Channel 7 surface reflectance images
- Surface reflectance quality image
- Orbital coverage
- Number of Observations

The MOD09 product is available in two spatial resolutions:

- MOD09GQK (250 m resolution): 250 MB – Channel 3 to Channel 7 data is excluded
- MOD09GHK (500 m resolution): 150 MB

In this report, MYD09GHK imageries were used.

The abbreviation “MYD” is used with reference to MODIS products from the sensor on-board the AQUA platform as opposed to “MOD” used to refer to MODIS data from the sensor on the TERRA platform.

The MODIS surface reflectance product is used to produce the Vegetation Index product. To eliminate the effects of clouds, aerosols and varying view- and sun angles, composites are made of products. 16-Day composites are made of the vegetation product.

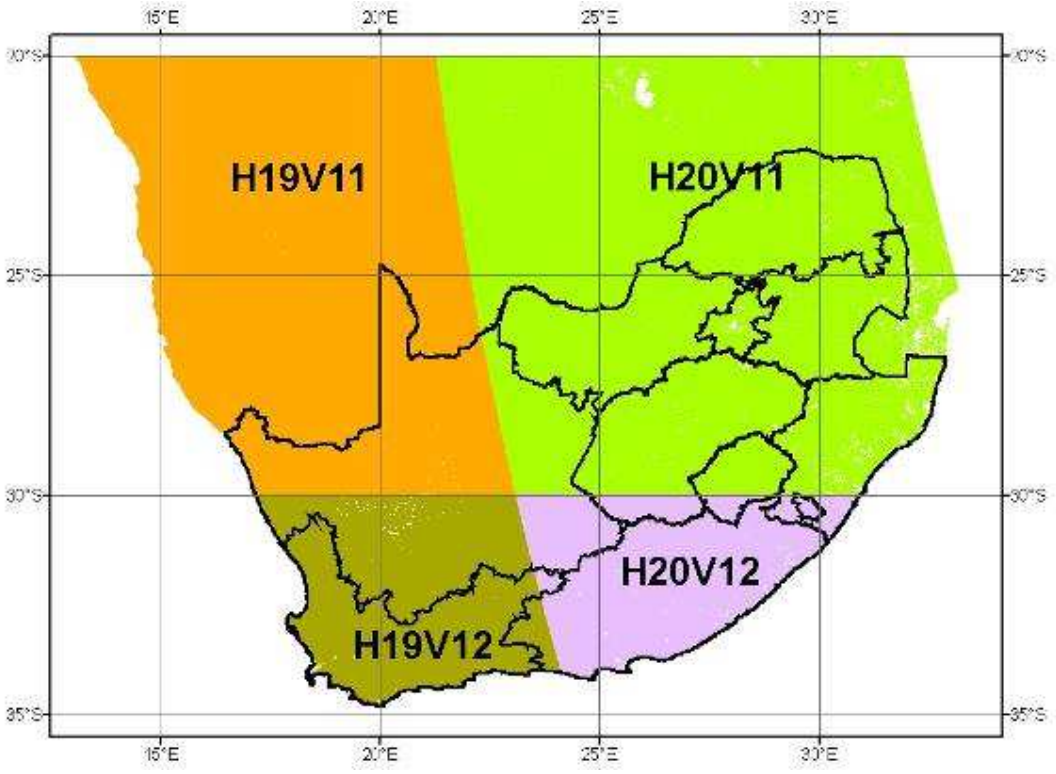

Figure 3.4 MODIS tiles covering South Africa.

The MODIS vegetation index 16-day composite product is labeled: MOD13. These Vegetation Index products are available in three spatial resolutions. When downloaded, the products per tile have the following sizes (in order of decreasing resolution)

- MOD13Q1 (250 m, resolution): 495 MB
- MOD13A1 (500 m resolution): 123.9MB
- 3A2 (1 km resolution): 31MB.

A MOD13 tile consists of:

- NDVI image
- EVI (enhanced Vegetation Index) image

- NDVI quality image
- EVI quality image
- 16-day average relative azimuth angle
- 16-day average sun zenith angle
- 16-day average view zenith angle
- 16-day average mid-infrared
- 16-day near infrared image
- 16-day red image
- 16-day blue image

When converted into GeoTiff format, each of the abovementioned in the case of the 1 km resolution product is about 3.1 MB in size. The NDVI and EVI values are scaled between 1 and 10,000 for 12-bit radiometric accuracy. The pixel values in all the bands are in signed 16-bit integer format while the quality checks are in unsigned 16-bit integer format.

Table A2 (Appendix I) shows the quality grid information for the MODIS vegetation indices. The quality assessment grid values must be related to 16 bit binary values and from that the quality information can be deducted. For example, a value of 38981 means that the following bits have been turned to 1 while the others are still zero: 15, 12, 11, 6, 2 and 0. The fact that bit 0 is turned to 1 indicates that there is cloud contamination. When bits 11 and 12 are turned to 1, it means that the pixel covers a land surface.

Figure 3.5 shows an extract from a 1-km resolution 16-day composite NDVI and a 250 m resolution 16-day composite NDVI for April 2002. The cloud contamination for this period is clearly visible as the islands with different values. The quality mask (Figure 3.6) indicates the entire area as being composited with the CA-MVC method. Over the areas perceived contaminated by clouds, the mask does acknowledge this fact. Therefore, the first bit of the sixteen quality bits is turned to 1.

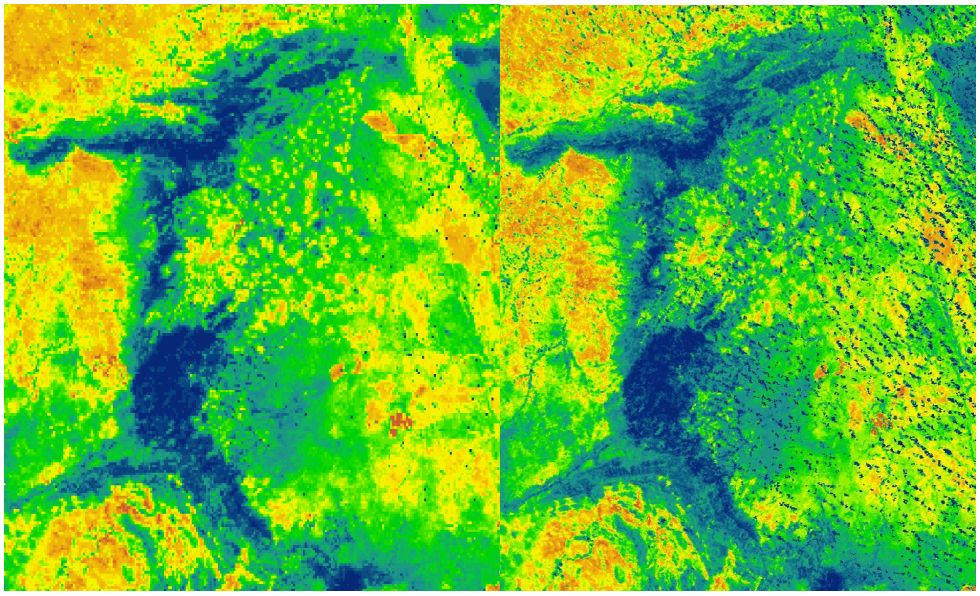

Figure 3.5 Cloud contamination visible on 1 km resolution (left) and 250 m resolution (right) NDVI image for the north eastern parts of South Africa.

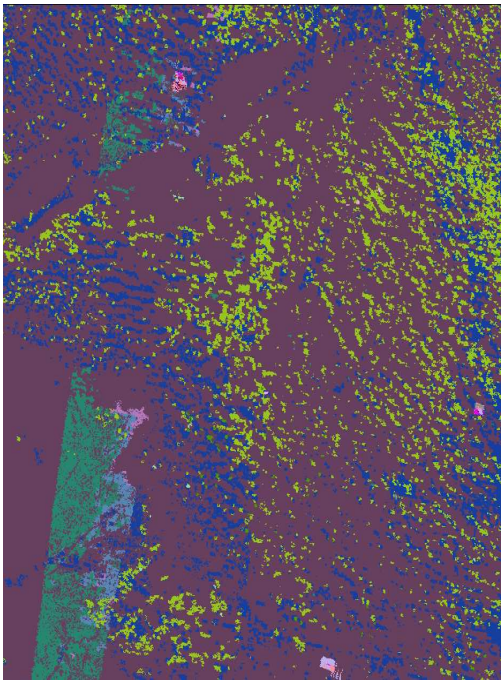

Figure 3.6 Quality control image for the 250 m NDVI product indicating areas of cloud contamination in yellow and blue.

Some known issues that have been reported at the Land Data Operational Product Evaluation (LDOPE, 2004) facilities are the following:

- Unreliable cloud information propagated into MOD13 QA bits.
- Stripes due to mixed clouds found in some MOD13A1 tiles.
- BRDF method not currently used in making NDVI and EVI.
- Blue (band 3) reflectance striping propagating into EVI under high atmospheric aerosol loading
- Speckles observed in 1 km 16-day EVI.

It is also acknowledged that the VI's under clouds remain unreliable and that the quality assessment bits should be examined (Didan and Huete, 2002).

Atmospheric data for use during Atmospheric correction in this report were the MYD07 (atmospheric water vapor profile) and MYD04 (atmospheric aerosol) products. The MYD07 product contains temperature, moisture and geo-potential height profiles at 20 standard pressure levels as well as total atmospheric water vapor and total atmospheric ozone (MYD07 Product Description, 2005). The MYD04 product contains data for the optical thickness at various wavelengths (MYD04 Product Description, 2005). Data that were acquired from the Atmospheric Water Vapor Profile product (MYD07) were the daily total precipitable water content of the atmosphere as well as total Ozone. Aerosol optical thickness values were obtained from the Aerosol product (MYD04).

The reason MODIS atmospheric data were used for this report is twofold.

Firstly, MODIS atmospheric data is used to apply the atmospheric correction to the MODIS red and near-infrared bands to obtain surface reflectance product, MOD09 (MODIS web, 2005). Secondly, on certain days, the MODIS sensor on the AQUA platform passes over the same area as the AVHRR sensor on NOAA-16during the afternoon, making it possible to obtain atmospheric data for the area covered by the AVHRR sensor within a short time of image acquisition.

The choice of total column precipitable water content, ozone and aerosol optical thickness at 55 μm as input variables for atmospheric correction is motivated by the reported findings regarding the importance of the influence of these constituents on the red and near-infrared reflectance. Furthermore, the 6S code can be used with these data as atmospheric input variables.

Historically, daily total ozone values are available for the entire globe, for the period of AVHRR data availability in a 1°X1.5° resolution. This data have been recorded by the Total Ozone Mapping Spectrometer (TOMS), a sensor focusing on ozone retrieval. This sensor have been flown by NASA on three different platforms since 1979 (TOMS, 2005)

Total precipitable water content data is available from the National Center for Environmentel Prediction (NCEP) on a six-hourly basis and a spatial resolution of 2.5° by 2.5°. This data is available since 1948 (NCEP Reanalysis, 2005).

Aerosol optical thickness at 55 μm is more difficult to obtain. The MODIS aerosol product used for this report is available since 2000. Prior to that, TOMS data is available since 1979. However, the AOT values are only available for the 380 μm wavelength. The Global Aerosol Climatology Project (GACP, 2005), which forms part of the NASA Radiation Sciences Program and the Global Energy and Water Cycle Experiment (GEWEX) is in the process of developing a 20-year aerosol climatology over land surfaces. This data is, however, not yet available.

Two tools available for MODIS data were utilized to handle the MODIS HDF data and deduce information thereof. These are:

- The MODIS Re-Projection Tool – used for the surface reflectance and NDVI products (MOD09 and MOD13). It is implemented to project, resample and export land surface product data.
- HDF-Look software – used to view, project and export MODIS atmosphere products data (MYD04 and MYD07). HDF-Look software operates on CYGWIN, a UNIX simulator for WINDOWS.

All data for MODIS used in this report were collection 4 products. These data were obtained from the EOS data gateway. Three types of MODIS data were downloaded. These included the 500 m resolution MODIS NDVI composites for 2002 (MOD13A1), 500 m resolution surface reflectance data (MYD09GHK) for specific days during which AQUA and NOAA-16 overpasses coincided with little or no cloud cover over the area of interest, and also 5 km resolution atmospheric products (MYD 04 and MYD07) for MODIS during the days for which the surface reflectance data was acquired. Data were downloaded for the tile that covers the area of interest (H20V11 – figure 3.4).

The 500 m resolution MODIS land surface product data were resampled through bilinear interpolation to an AVHRR-equivalent resolution of 1 km using the MODIS Re-projection Tool before any values were extracted. It was then exported into GeoTiff format with a Plate Carree projection. The HDF-Look software was used to obtain the atmospheric data values for each of the 17 points to be used during the atmospheric correction algorithm. The atmospheric data products cannot be handled with the MODIS Re-Projection Tool.

3.4 Spatial and temporal differentiation in the NDVI for the two sensors

The 16-day composite AVHRR and MODIS NDVI values for the entire year 2002 were extracted for each of the 17 polygons distributed over the Umkhanyakude node (Figure 4.2). For the MODIS NDVI composite product the accompanying quality assessment images were evaluated for each 16-day periods during 2002. The quality assessment values indicated throughout 2002 for all the 16-day composites used over the area of interest that the quality of the NDVI composites was acceptable and that the CA-MVC method was applied to make composites of the data. Furthermore, no cloud contamination was indicated.

The MODIS and AVHRR 16-day composite NDVI values were plotted together on a time-series graph for each polygon to investigate the difference throughout 2002 between these values. The Mean NDVI values for both sensors were also plotted against each other for every point.

Firstly, for all the 17 points together and secondly, for every point separately, a regression analysis was done between the AVHRR and MODIS 16-day composite NDVI for 2002 yielding linear models in the following format:

$$(NDVI_{MODIS}) = A + B * (NDVI_{AVHRR})$$

A linear relation was noticed between the slope and the intercept of the equation at each point and the mean NDVI value at the point. In order to derive a more robust method to express the relation between the MODIS NDVI and the AVHRR NDVI at all the points separately, a new equation for each point was estimated through the relationship between the mean of the AVHRR 16-day composite NDVI value at the point and the slope and intercept for the linear model equation at that specific point.

Daily imageries for specific dates throughout 2003 were used to test the accuracy of the methods for the 17 polygons. Six entirely cloudless scenes were identified to test the methods over the entire Umkhanyakude node in terms of all cells separated according to the mean AVHRR NDVI.

3.5 Effect of atmosphere and BRDF on relation between AVHRR and MODIS NDVI

For 26 days during 2003 when near simultaneous overpasses of AQUA and NOAA-16 coincided with little or no cloud cover over the area of interest, the red and near infrared channel values for both sensors were extracted for the polygons at each of the points. These comprised the surface reflectance values in the case of MODIS and the TOA reflectance values in the case of AVHRR.

It was decided not to do corrections for the BRDF for daily NOAA imagery based on the following facts:

- The daily MODIS 16-day composite NDVI products and reflectance imagery obtained had not been corrected for sun-sensor-target geometry.
- Corrections for the BRDF within 6S and in general are not advised for heterogeneous targets.
- The influence of the change in solar zenith angle between summer and winter is the same for both sensors.
- BRDF is land-cover specific and over a period of roughly 20 years land-cover will change over some areas, necessitating the recalculation of parameters for the model being used for correction of it.

The Atmospheric Correction Code 6S was used to do correction for atmospheric influences. It was compiled on a FORTRAN 77 compiler called MinGW (MinGW 3.1.0 for WIN32). The resulting executable and input files were called from DOS command line on a Personal Computer with a WINDOWS XP operating system. Figure 3.7 is an example of an input file for the near-infrared channel of the AVHRR.

```
0                           (Sun-Sensor_Target geometry and date follows)
23.6 302.0 50.0 147.0 2 12
8                           (USER'S  MODEL)
2 0.251                     (UH2O(G/CM2) ,UO3(CM-ATM))
4                           (AEROSOLS MODEL)
0.25  0.25  0.25  0.25      (% OF:DUST-LIKE,WATER-SOL,OCEANIC,SOOT)
0                           (NEXT VALUE IS THE AERO. OPT. THICK. @550nm)
0.043                       (AERO. OPT. THICK. @550nm)
-0.2                        (TARGET ALTITUDE IN KM)
-1000                       (SATELLITE CASE)
1                           (USER'S WLINF-WLSUP, followed by spectral response function in 0.0025 micron steps)
0.668 1.008
0.00001 0.000045 0.00008 0.00008 0.00012 0.00016
0.000205 0.000455 0.00066 0.00182 0.00365 0.00548
0.010475 0.01547 0.026465 0.037645 0.03783 0.094665
0.1515 0.1871 0.2227 0.2915 0.3232 0.3549
0.4112 0.45175 0.4923 0.55425 0.68155 0.7469
0.7959 0.8449 0.8808 0.86285 0.8698 0.86325
0.8496 0.85355 0.8575 0.88095 0.9044 0.9316
0.9588 0.97515 1 0.995 0.99 0.9874
0.9848 0.9881 0.98285 0.9626 0.9626 0.9587
0.9548 0.9569 0.959 0.9641 0.9692 0.9723
0.9754 0.9789 0.9795 0.97885 0.9782 0.97605
0.9739 0.9717 0.97025 0.9688 0.9669 0.965
0.9541 0.9476 0.9411 0.93465 0.9219 0.9156
0.9099 0.90905 0.9082 0.90905 0.9147 0.9242
0.93075 0.9373 0.9427 0.94135 0.94 0.9337
0.9274 0.911 0.904 0.897 0.8909 0.89355
0.8962 0.9022 0.9082 0.9218 0.92565 0.9295
0.9247 0.91635 0.908 0.89755 0.8871 0.8623
0.85165 0.841 0.8278 0.8146 0.7988 0.7941
0.7894 0.7872 0.785 0.7863 0.785 0.7837
0.76415 0.76415 0.7446 0.6898 0.6898 0.5751
0.4604 0.4604 0.31975 0.31975 0.1791 0.1791
0.10753 0.10753 0.10753 0.03596 0.03596
1
1 1 0.5                         (non homogeneos case for vegetation and 1km radius)
-0.124                          (negative Apparent reflectance input at satellite for atmospheric correction)
```

Figure 3.7 Example of input file for 6S.

The input data for the code consist of the sun- and sensor zenith and azimuth angles, date, water vapor content (in $g.cm^{-2}$), subdivision of aerosol into different types (dust-like, water-soluble, soot, oceanic), aerosol optical thickness at 55 μm, target altitude, lower and upper spectral bounds of the satellite sensor channel, normalized spectral response of the specific satellite sensor channel in steps of 0.0025 μm, target reflectance characteristics, type of surroundings (for example vegetation or sand), radius of target and the TOA reflectance for the specific channel. For each channel, a separate input file was created per site per day and results were also given in separate text files.

Various sources were utilized to obtain the input data needed for the 6S atmospheric correction code. The normalized spectral response function for each of the AVHRR channels was interpolated from data available via the International Satellite Cloud Climatology Project (ISCCP, 2005). The atmospheric data was obtained from the MODIS atmospheric products (MYD04 and MYD07) while the 32-bit AVHRR data from the ISCW was used for the TOA reflectance. The default aerosol composition model was used as only the optical thickness at 55 μm was available as input data and no further information was available from the atmospheric products. Because no profile data was available for ozone, the total column precipitable water and the total column ozone were

provided as inputs while the model utilizes a standard atmospheric profile to establish the influence of these constituents together. A further consideration in this regard was that surrogate data should be available since 1985 and that the method and data gathering and input process should not be exhaustive.

The uncorrected and corrected NOAA AVHRR red and near-infrared channel responses and NDVI values were compared to the MODIS red and near-infrared responses and NDVI to establish whether a more stable relationship can be obtained between the corrected AVHRR data and the MODIS data than with the uncorrected AVHRR and MODIS data.

3.6 Effect of image miss-registration

To formulate an idea of the influence of miss registration of pixels on the values extracted per polygon for all the sites over this specific area, an NDVI image was created from NOAA-16 AVHRR data. The image was shifted one pixel at a time and values were extracted for the points used with the composites. The differences in the NDVI values between the various images for all of the points were used to formulate an idea of an increase in error with increasing miss-registration.

4. CRITICAL COMPARISON OF AVHRR- AND MODIS-DERIVED NDVI

4.1 Temporal and spatial characteristics of the relation between NDVI for MODIS and AVHRR

The mean AVHRR and MODIS NDVI calculated at each point was used as an indication for the relation of the mean NDVI with land-cover. Both the AVHRR and MODIS NDVI increased from the Subsistence Dry-land Agriculture land-cover class through the Grassland and Bushland classes to the Forest land-cover class (Figure 4.1). This is an indication of the land-cover dependence of the mean NDVI from both sensors.

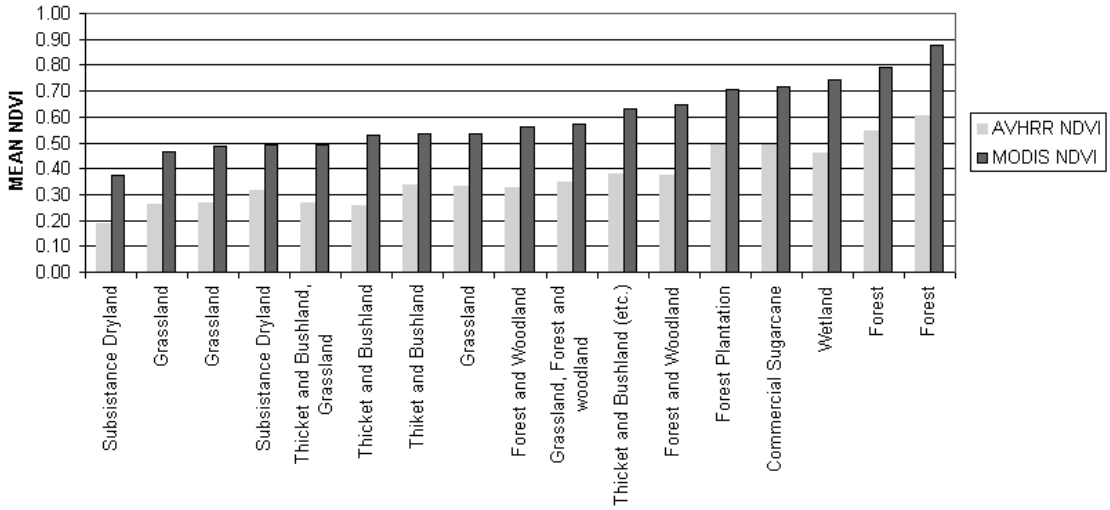

Figure 4.1 MODIS and AVHRR for the 17 points indicated per land-cover classes, in order of increasing mean MODIS NDVI.

Time-series graphs for the 17 points of the 16-day NDVI composites for both sensors throughout 2002 were compared. The similar responses of the NDVI composite values of both sensors in reaction to the temporal distribution of rainfall were evident. Both sensor NDVI composite values indicated decreased activity during autumn and winter, while the values increased early in spring after good rain. During October, when it was dry, values decreased, to increase again at the end of the year as normal rain returned to the area. The AVHRR NDVI values were always lower than the MODIS NDVI values (Figures 4.2 to 4.4) throughout the year, for each point over all the land-cover classes.

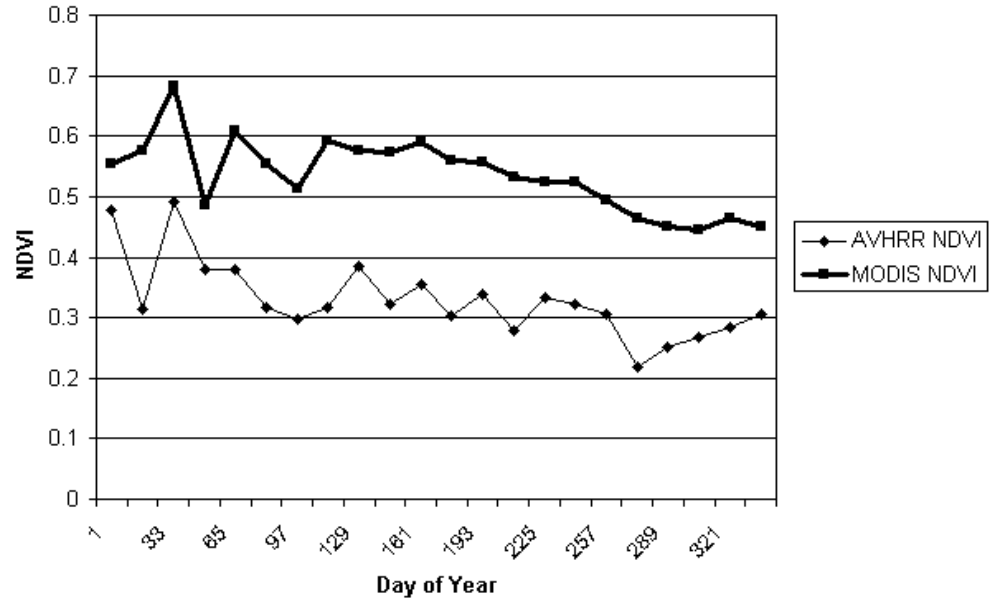

Figure 4.2 Time series for AVHRR and MODIS NDVI for a grassland site in Node 4 during 2002.

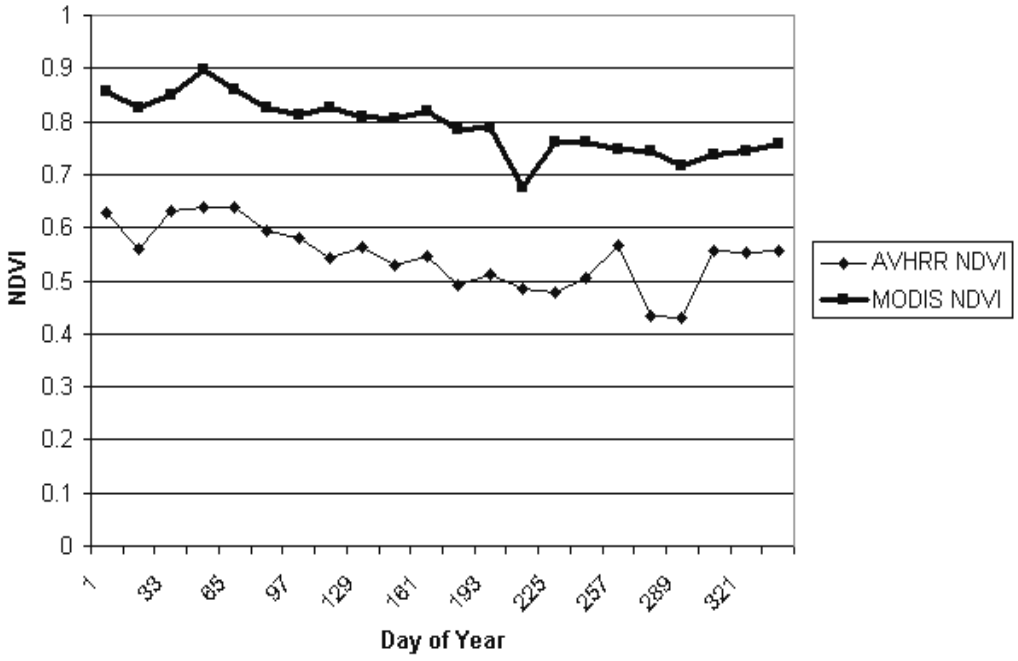

Figure 4.3 Time series for AVHRR and MODIS NDVI for a forest site in Node 4 during 2002.

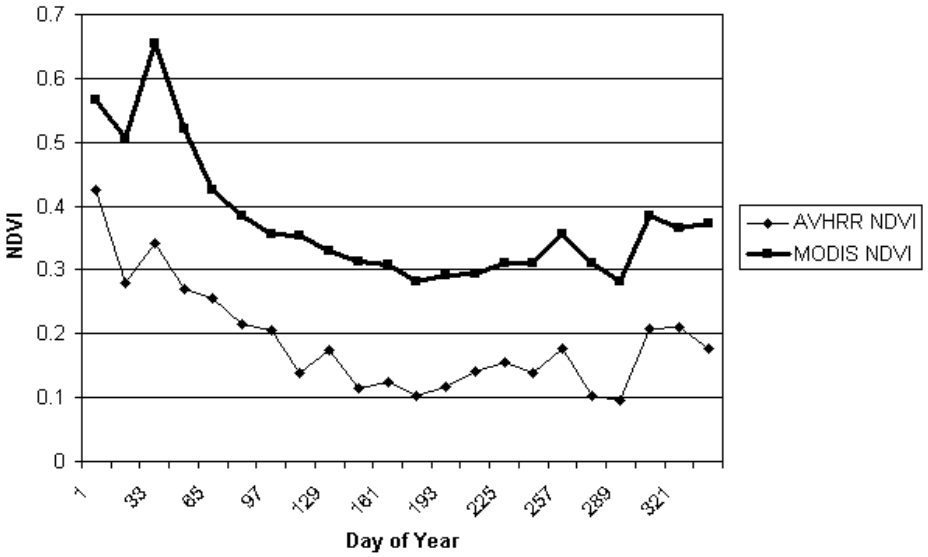

Figure 4.4 Time series for AVHRR and MODIS NDVI for an area under temporary subsistence cultivation in Node 4 during 2002.

A linear relation between the AVHRR and MODIS NDVI values is supported by figure 4.1 to figure 4.4. The sites with higher mean MODIS NDVI values also had higher mean AVHRR NDVI values. Furthermore, sites where the MODIS NDVI had a higher standard deviation also exhibited a higher AVHRR NDVI standard deviation (Figure 4.5).

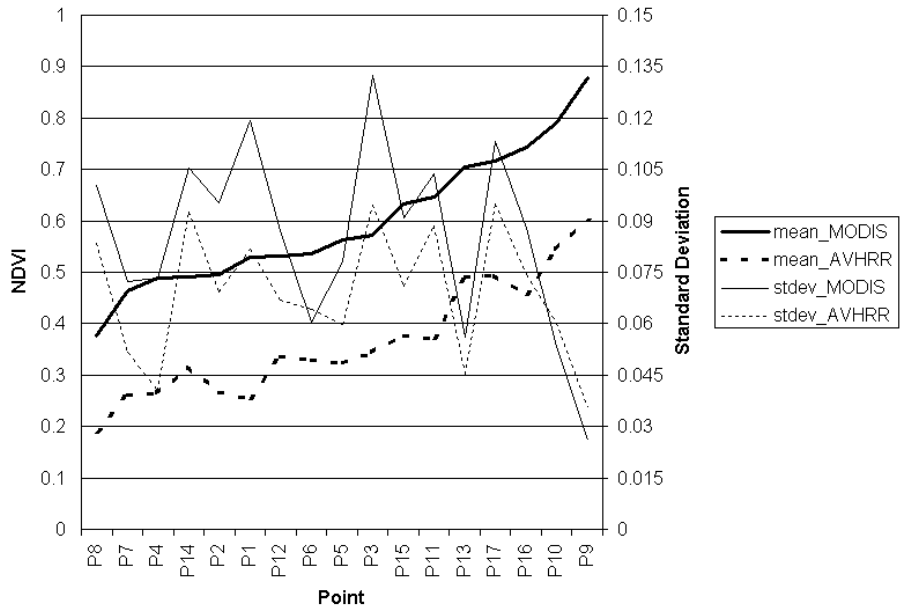

Figure 4.5 Mean and standard deviation of AVHRR- and MODIS NDVI 16-day composite values for all the points for 2002.

Overall, an R-squared value of 0.95 was found between the mean NDVI composite values of AVHRR and MODIS for all sites (Figure 4.6).

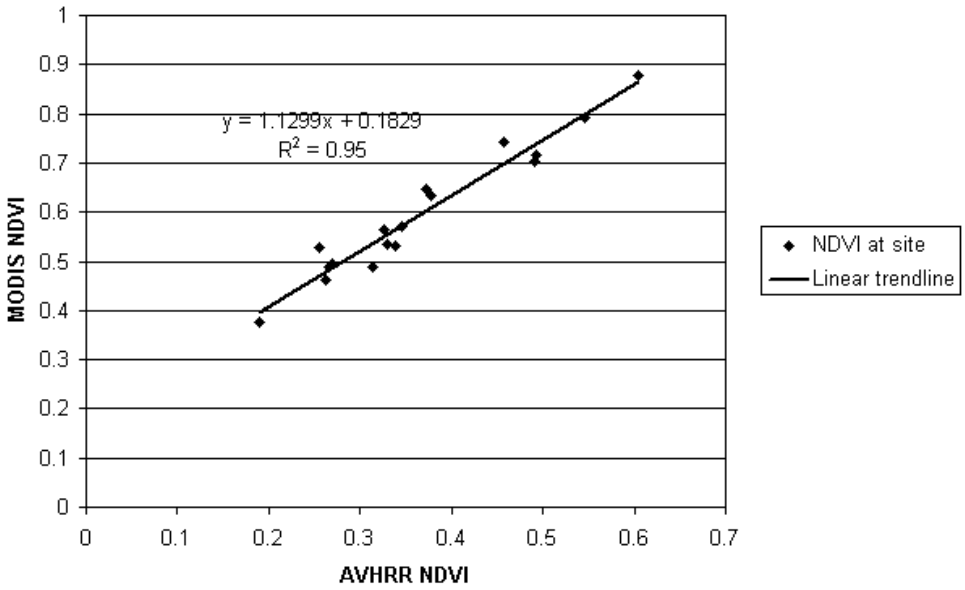

Figure 4.6 The linear relationship between the annual mean AVHRR and MODIS 16-day composite values at every point.

The characteristics of the difference between the MODIS and AVHRR composite values throughout 2002 at all the sites are indicated in figure 4.7 which is a box plot based on the difference between the NDVI values for MODIS and AVHRR for each point. As for figure 4.1, the points were sorted from left to right according to increasing average MODIS NDVI values. The median difference ranged between 0.24 and 0.3. The inter quartile range (IQR) was never larger than 0.08, but the adjacent value ranges could be as large as 0.2. Furthermore, larger differences were observed over areas with higher NDVI values than over areas with lower NDVI values.

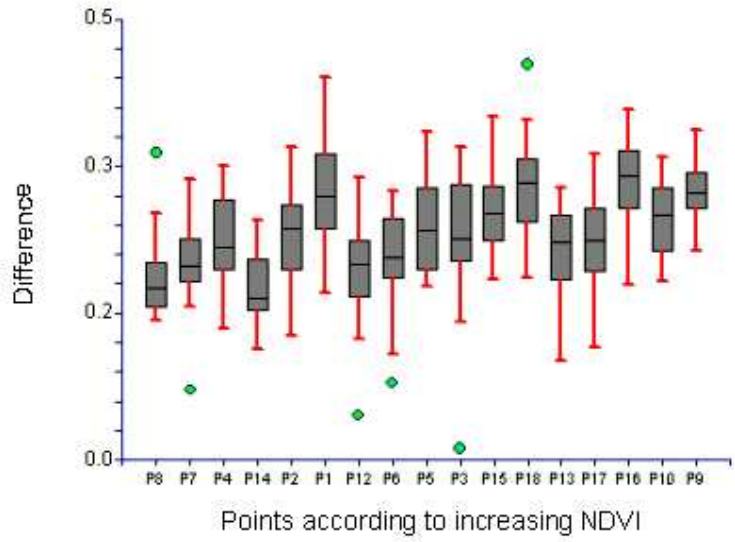

Figure 4.7 Box plot of difference between the composite NDVI values of MODIS and AVHRR for all points during 2002 (Dots indicate mild outliers).

For all the periods, at each of the seventeen sites, the regression model between the AVHRR and MODIS were calculated and given in the following format:

(AVHRR NDVI) = A + B * (MODIS NDVI)

The value of the intercept (A) ranged between 0.16 and 0.64 and the value for the slope (B) ranged between 0.4 and 1.4 (Figure 4.8)

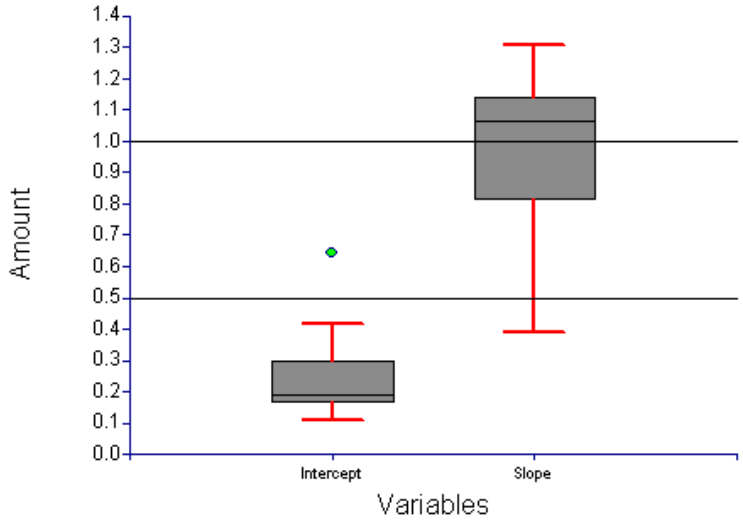

Figure 4.8 Box plot indicating the variation in the slope and intercept for the separate linear regression models for all the points.

Furthermore, the R-squared value between the AVHRR and MODIS NDVI per site varied between 0.29 and 0.87 (Figure 4.9). The lowest value was for a forested area (with a high mean NDVI), 0.29, while the highest value of 0.87 was for an area under dry-land subsistence cultivation (with a low mean NDVI).

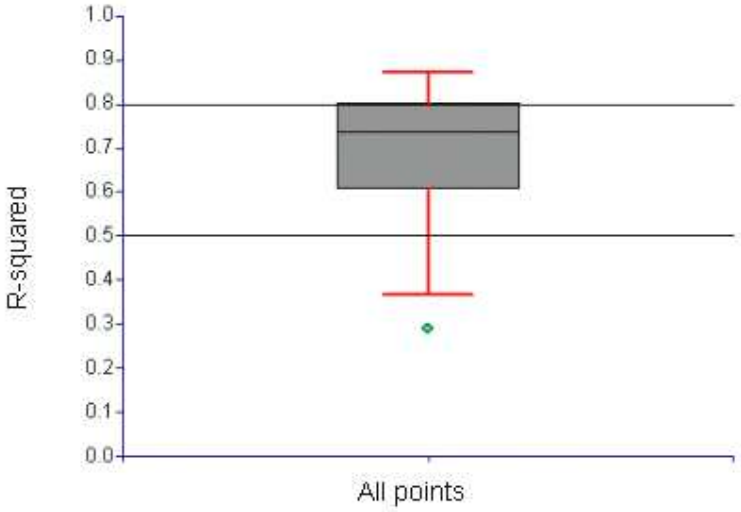

Figure 4.9 Range in R-squared values for the linear models used to describe the relation between the AVHRR and MODIS at each site.

The possibility of different linear models describing the relationship between the AVHRR NDVI values and MODIS NDVI values could be implied by the varying nature of the slope, intercept and R-squared values (Figure 4.8 and 4.9) obtained over the 17 points covering various land-cover types

The stratification of the data into different NDVI classes became an option. However, stratifying data and merging it together again could lead to visible spatial discrepancies in NDVI imagery. A robust method to estimate the values for the slope and the intercept of each site, without separating the data, was investigated. It was found that the intercept (A) and slope (B) of the model calculated for each point were correlated to the mean NDVI value calculated for that point from the composite NDVI values for the entire year 2002 (Figure 4.10 and Figure 4.11).

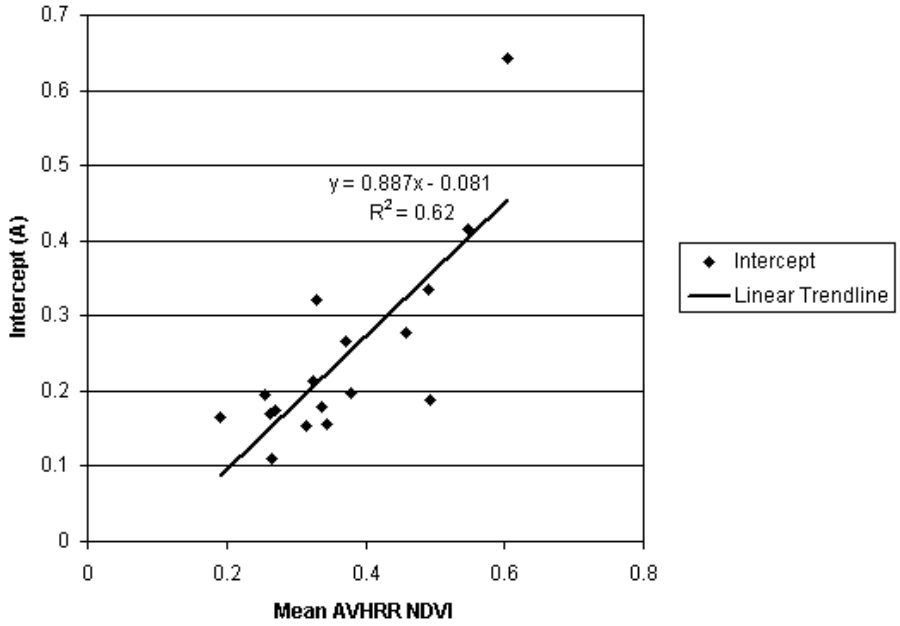

Figure 4.10 Linear relation between the intercept (A) of the regression model between AVHRR and MODIS NDVI and the mean AVHRR-derived and the mean NDVI for each site.

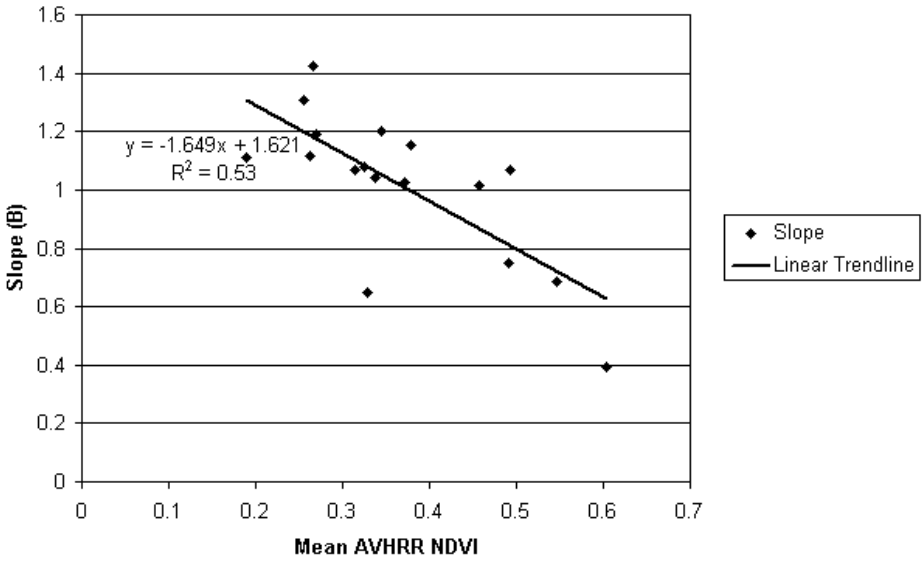

Figure 4.11 Linear relationship between the slope (B) of the regression model between AVHRR and MODIS NDVI and the mean AVHRR-derived NDVI at each site.

A linear model for the relation between AVHRR and MODIS NDVI values, for each site, related to the average AVHRR NDVI value, was proposed. The intercept (A) of the model at each point was related to the mean AVHRR NDVI in the following manner:

$$A = -0.081+(0.887*(NDVI_{Mean\ AVHRR})$$

While the slope (B) of the model at each point was related to the mean AVHRR NDVI in the following manner:

$$B = 1.621+(-1.649*(NDVI_{Mean\ AVHRR}))$$

Alternatively, the linear model derived from all the data was still an option.

The two methods so far were:

$$NDVI_{MODIS} = A + B * NDVI_{AVHRR} \qquad W1$$

where A = 0.087 and B = 1.307

and

$$NDVI_{MODIS} = A + B * NDVI_{AVHRR} \qquad W2$$

where A and B are functions of the mean AVHRR NDVI at the specific point.

In order to test the two methods, days during 2003 when little or no clouds were detected over the area of interest were identified. Given the climate of the area of interest as well as the standard set to consider a specific scene, a very small fraction of days were considered allegeable for daily data. The period considered was from January to December 2003. Special emphasis was placed on the retrieval of clear pixel values and as a result only days with more than 80% clear pixels over the area of interest were considered. Furthermore, before data were extracted for a specific polygon, a visual inspection was also implemented to verify that the pixels are clear as far as can be ascertained. The cloud mask was examined for AVHRR data and the quality assessment image was considered for MODIS data. Initially, data were collected for all scan angles from 0° to 65°. However, it became clear that the response of the red channel of the AVHRR was impacted on when scan angles were high. Independent of the relative azimuth angle between the sun and the satellite, the red channel response soared at high view zenith angles (Figure 4.12). Furthermore, the geometric distortion at high view zenith angles is the reason that the automated processing at the ISCW ignores data from these angles. This is a reason why data for AVHRR or MODIS view-angles larger than 45° were omitted. Only 26 days proved satisfactory for inclusion into the daily data analysis.

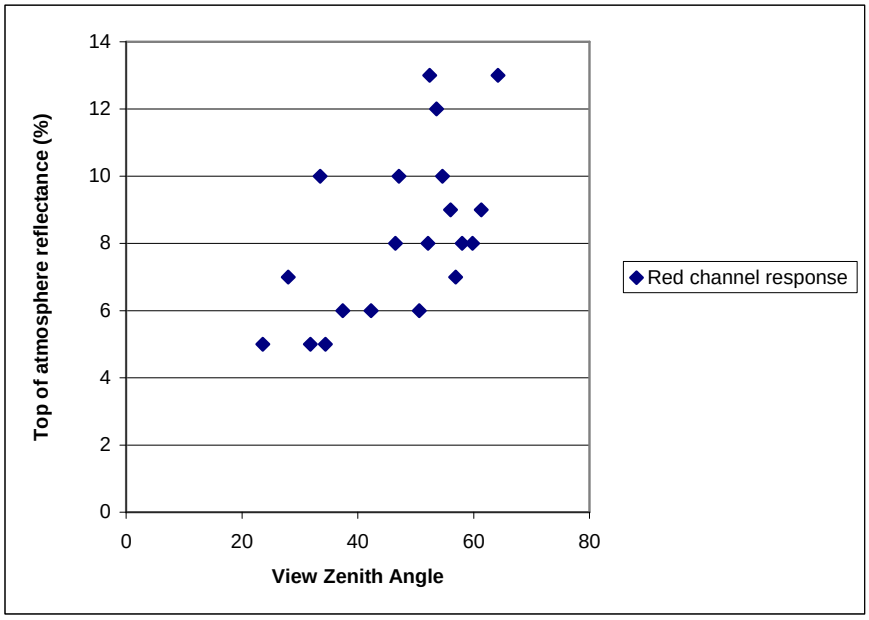

Figure 4.12 Red channel response as influenced by satellite view zenith angle.

For each point, MODIS-equivalent NDVI values were estimated from the selected daily AVHRR NDVI values by means of method W2 and W3. The difference in terms of the root-mean-square error of each method is indicated in figure 4.13

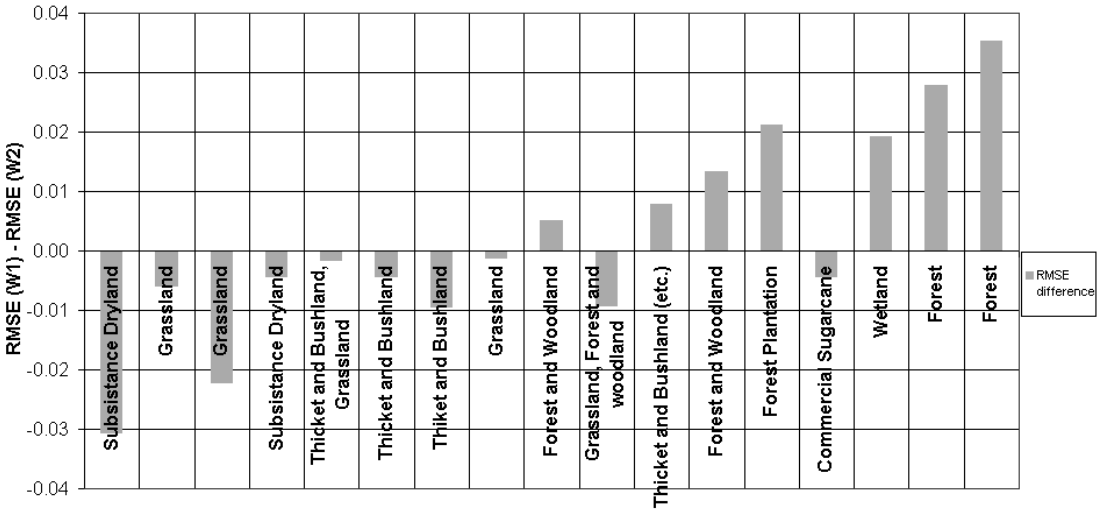

Figure 4.13 Difference in RMSE for the two methods W1 and W2 for all 17 points situated at various land-cover classes, sorted in order of increasing mean MODIS NDVI.

The root-mean-square error over all the points for W2 was 0.032 NDVI units smaller than for W1. What is encouraging is that this method (W2) can be applied with only the mean AVHRR NDVI value at a point as input to estimate the slope and intercept of the model for each point. It can however be seen that W2 performed slightly worse than W1 over the areas with a lower mean NDVI and vice versa over areas with a high mean NDVI value. The reason for this is that a trend in the root-mean-square error with the application of W1 was removed (Figure 4.14).

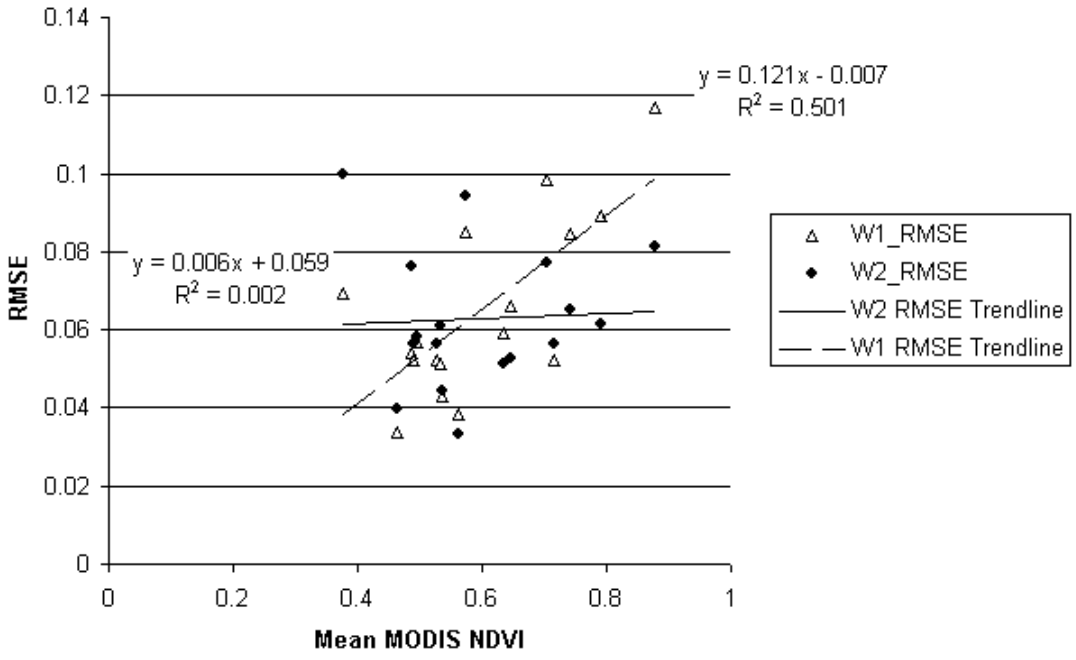

Figure 4.14 Root-mean-square error resulting when estimating a MODIS-equivalent NDVI from the daily AVHRR NDVI as a function of the mean MODIS NDVI at all 17 points.

For six cloudless scenes representative of all four seasons through 2003, the MODIS-equivalent NDVI values were estimated through methods W1 and W2. Figure 4.15 shows the MODIS and the MODIS-equivalent NDVI images as calculated through the W1 and W2 methods. To get an indication of how applicable the two methods were over the range of NDVI values and hence the range of land-cover classes, the root-mean-square error values were calculated for areas with different mean AVHRR NDVI values separately (Figure 4.16). Imageries for all six dates were used and all pixels in the Umkhanyakude node were used to derive the statistics. While the root-mean-square error over the entire

node for both methods respectively were just below 0.05 NDVI units, it can be seen that the root-mean-square error values for W1 ranged between 0.027 and 0.07 with increasing mean AVHRR NDVI, while the root-mean-square error for W2 over the entire range of NDVI classes was stable around 0.05. It follows that method W2 is equally suitable over the range of mean AVHRR NDVI values and hence land-cover classes, while method W1 becomes less reliable towards the land-cover classes with the higher mean AVHRR NDVI. For this reason it was decided that method W2, or at least any other method that incorporates the stratification of imagery into different mean long-term NDVI classes or land-cover classes, will yield more consistent results over a large area.

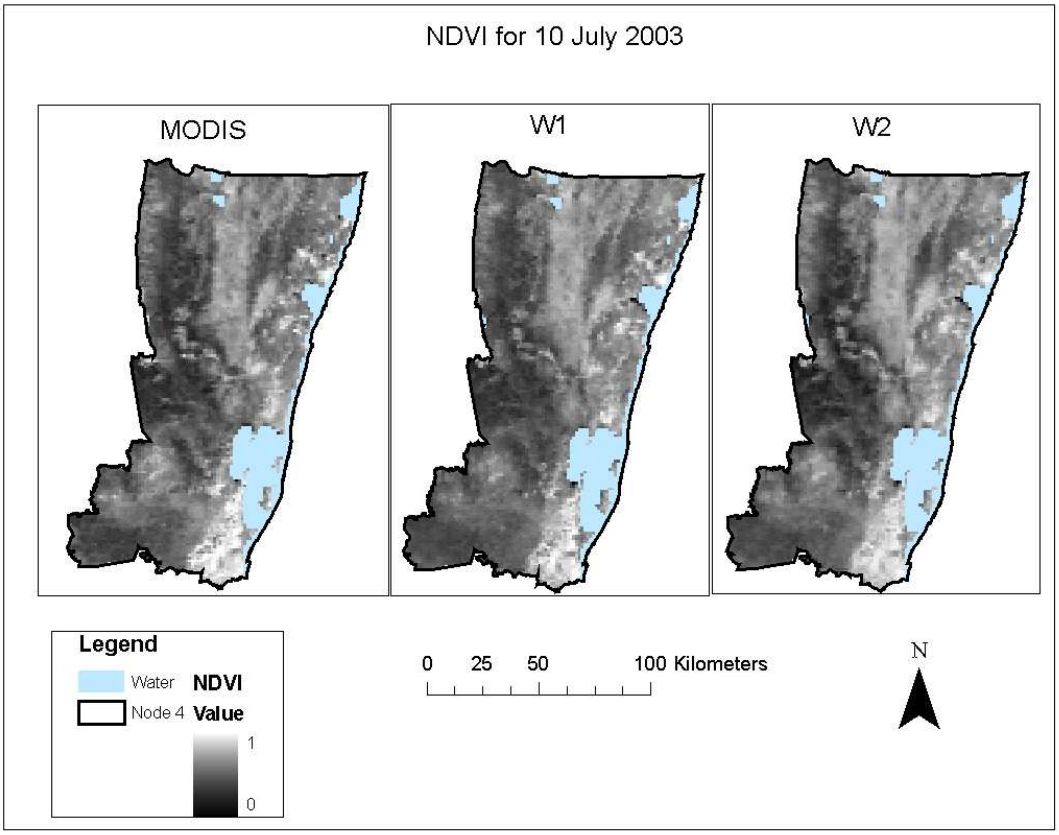

Figure 4.15 MODIS NDVI and MODIS-equivalent NDVI image as calculated with the W1 and W2 methods.

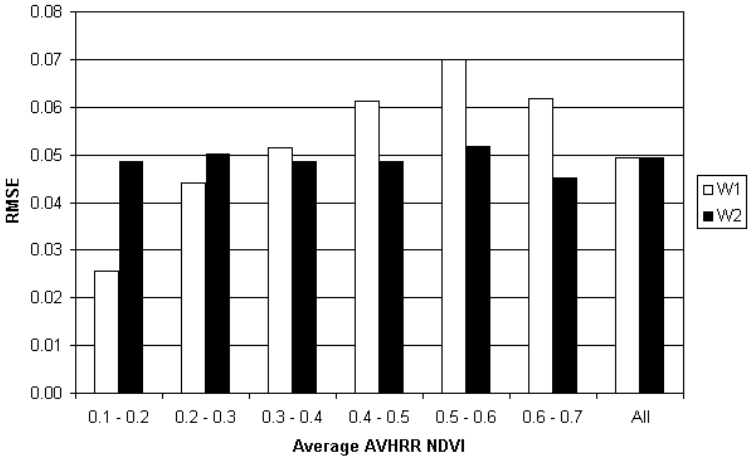

Figure 4.16 Root-mean-square error calculated over the entire Node 4 resulting from the use of methods W1 and W2 when estimating a MODIS-Equivalent NDVI from AVHRR NDVI for cloudless scenes.

4.2 Effects of atmospheric corrections and BDRF constraints on AVHRR data

Data were collected for all points for the 26 chosen days during 2003 as input to the 6S atmospheric correction code. These included the TOA reflectance from both channel 1 and channel 2 of the AVHRR, sun-view geometry variables and atmospheric data from the MODIS atmospheric products. Because some of the areas were covered by cloud on certain days, the mean amount of days for which data were collected per point were 22.5. For a specific point, these input data are indicated in table 4.1.

Table 4 1 AVHRR TOA reflectance and geometric data and MODIS atmospheric data for specific days in 2003.

DATE	AVHRR CH 1 Reflec-tance (unitless)	AVHRR CH 2 Reflec-tance (unitless)	Solar Zenith Angle (Degrees)	Solar Azimuth Angle (Degrees)	View Zenith Angle (Degrees)	View Azimuth Angle (Degrees)	Preci-pitable Water ($G.cm^{-2)}$	Total Ozone (Db)	AOT (55 µm)
2003/01/02	0.125	0.225	34	268	40	283	2	255	0.2
2003/01/13	0.103	0.164	29	274	6	280	3.3	260	0.21
2003/02/12	0.071	0.143	24	300	47	2	2	262	0.19
2003/02/28	0.070	0.156	32	301	17	81	4.1	260	0.18
2003/03/18	0.076	0.151	37	309	18	81	3.1	256	0.17
2003/04/03	0.088	0.171	47	309	20	281	2.8	258	0.21
2003/04/06	0.067	0.157	42	318	37	83	2.1	256	0.2
2003/04/29	0.102	0.172	56	313	34	282	1.9	256	0.18
2003/05/08	0.091	0.167	58	315	33	282	2.5	256	0.08
2003/07/10	0.088	0.168	60	322	23	282	1.3	268	0.09
2003/07/17	0.113	0.207	62	316	50	284	1.1	282	0.1
2003/07/18	0.104	0.186	61	319	38	283	0.7	274	0.18
2003/07/26	0.119	0.196	61	315	49	284	1.9	272	0.22
2003/07/27	0.102	0.181	59	318	36	283	1.3	270	0.14
2003/08/14	0.100	0.184	56	313	33	282	2.2	305	0.13
2003/08/23	0.105	0.184	53	311	31	282	1.7	274	0.14
2003/09/03	0.088	0.145	47	313	9	81	1.3	276	0.36
2003/09/04	0.088	0.140	45	315	28	82	1.6	277	0.34
2003/09/12	0.090	0.135	45	309	12	81	2.2	284	0.31
2003/10/10	0.095	0.136	37	298	36	82	2.7	284	0.51
2003/10/24	0.125	0.181	44	282	35	282	3	278	0.28
2003/11/04	0.083	0.141	37	280	7	80	3.5	287	0.24
2003/12/01	0.082	0.158	33	271	16	81	3.2	272	0.15
2003/12/11	0.079	0.144	29	271	36	82	3.2	273	0.18
2003/12/29	0.086	0.151	26	272	41	83	4.3	277	0.29

Precipitable water content revealed a seasonal pattern with high values during summer and low values in winter (Figure 4.17). In the 6S atmospheric correction code, the total precipitable water used for a tropical atmosphere is 3 $g.cm^{-2}$. AOT at 55 µm was the highest during spring and relatively lower during the rest of the year.

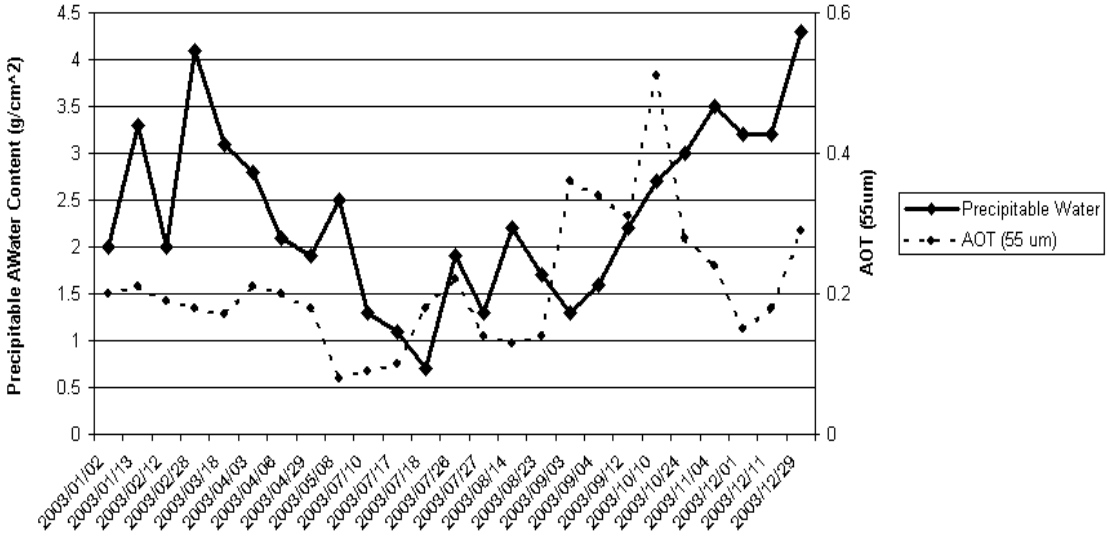

Figure 4.17 Total precipitable water content (g.cm^{-2}) of the atmosphere and aerosol optical thickness at 55 µm at a specific point during 2003.

The parameters shown in table 4.1 were used in the 6S atmospheric correction model. It can be seen that the model responded correctly to various amounts of precipitable water and aerosol optical thickness (AOT) in the atmosphere (Figure 4.18 to figure 4.20)

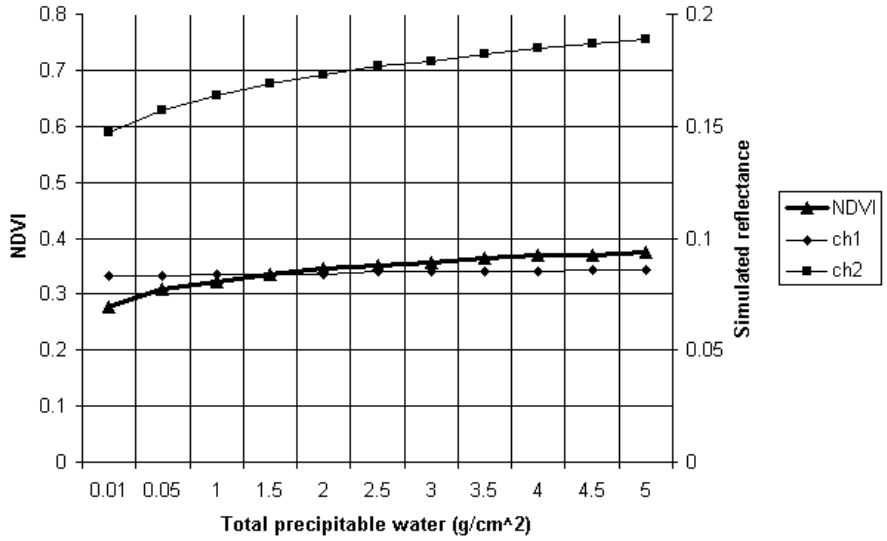

Figure 4.18 Adjustment of red (Ch 1) and near-infrared (Ch 2) AVHRR estimated surface reflectance and resultant change in NDVI, for constant input top of the atmosphere reflectance values, with increasing total atmospheric precipitable water content.

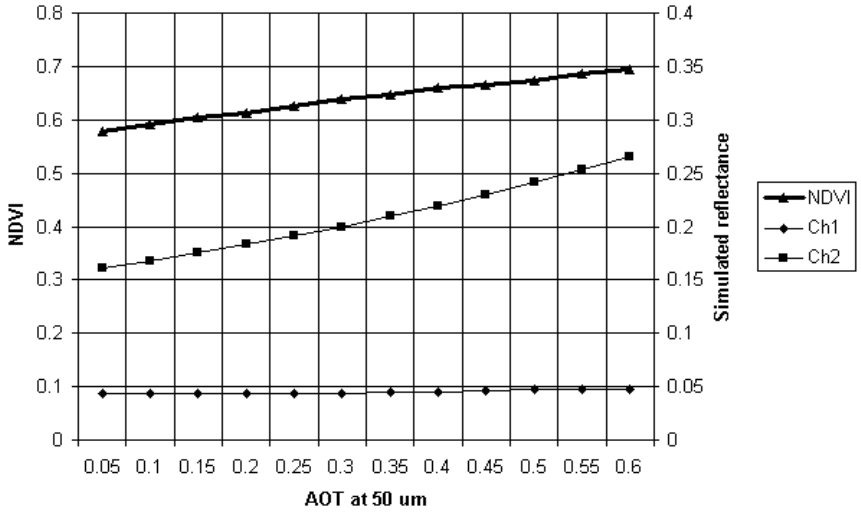

Figure 4.19 Adjustment of red (Ch 1) and near-infrared (Ch 2) AVHRR estimated surface reflectance and resultant change in NDVI, for constant input top of the atmosphere reflectance values, with increasing atmospheric optical thickness at 55 µm.

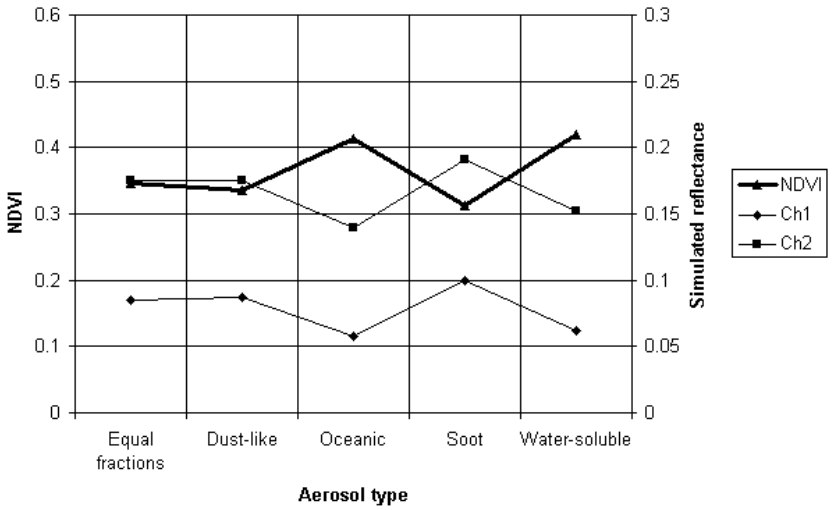

Figure 4.20 Adjustment of red (Ch 1) and near-infrared (Ch 2) AVHRR estimated surface reflectance and resultant change in NDVI, for constant input top of the atmosphere reflectance values, with different input aerosol type.

The change in AVHRR NDVI through the modelled change by the 6S model for the range of precipitable water amounts found on cloudless days (Figure 4.17) were 0.1 NDVI units (Figure 4.18). The same magnitude of change was possible for AOT at 55 μm variations found over the area on cloudless days (Figure 4.17 and 4.19). Uncertainty about the aerosol type can however also lead to errors in the same range as the corrections made (Figure 4.20).

Overall, from figures 4.18 and 4.19, it can be seen that the 6S model, with inputs as given in this report, handled the influence of the atmosphere in terms of direction of adjustment of the AVHRR NDVI correctly. However, in accordance to what has been reported in literature through spectrometer studies in laboratories, a linear model still has to describe the relation between AVHRR and MODIS NDVI values after atmospheric correction had been applied.

A linear regression analysis was done between all the daily atmospherically corrected AVHRR NDVI values and MODIS NDVI values. The results for the mean atmospherically corrected AVHRR value at each site and the mean MODIS NDVI for the site are indicated in figure 4.21. The R-squared value was 0.98 compared to 0.95 between the composite datasets of uncorrected data.

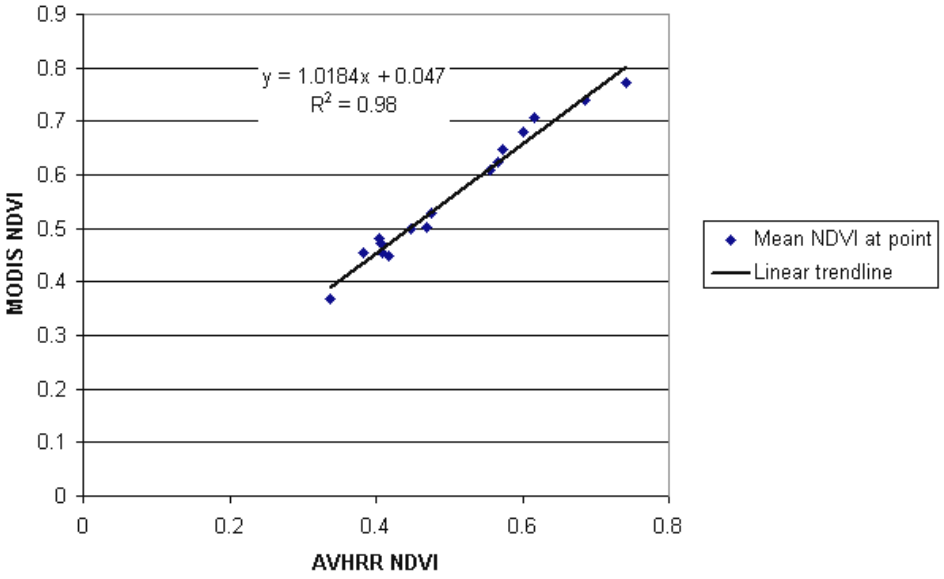

Figure 4.21 The linear relation between the mean atmospherically corrected AVHRR NDVI and MODIS NDVI values at every point.

The linear equation for all daily atmospherically corrected AVHRR NDVI and MODIS NDVI values had the following form:

$$NDVI_{MODIS} = 0.047 + 1.018 * NDVI_{AVHRR}$$

compared to the

$$NDVI_{MODIS} = 0.004 + 1.103 * NDVI_{AVHRR}$$

found in literature for agricultural vegetation (Steven *et al.*, 2003).

The same method as described earlier for the composite data was used to relate the mean AVHRR NDVI value at each site to the slope and intercept values of a site-specific linear model:

$$NDVI_{MODIS} = A + B * NDVI_{AVHRR\_Corrected\ for\ atmosphere} \qquad W3$$

where A and B are related to the mean AVHRR NDVI at the specific point.

This method was used instead of using a single linear equation between the atmospherically corrected AVHRR NDVI values and the MODIS NDVI values. Apart from it being the method proposed for the uncorrected data, the root-mean-square error involved in using this method was 0.015 NDVI units smaller than using a constant relationship.

The adjustment of the AVHRR NDVI for daily values during 2003 when using W3 is indicated for points situated in three land-cover types in figure 4.22 and figure 4.23.

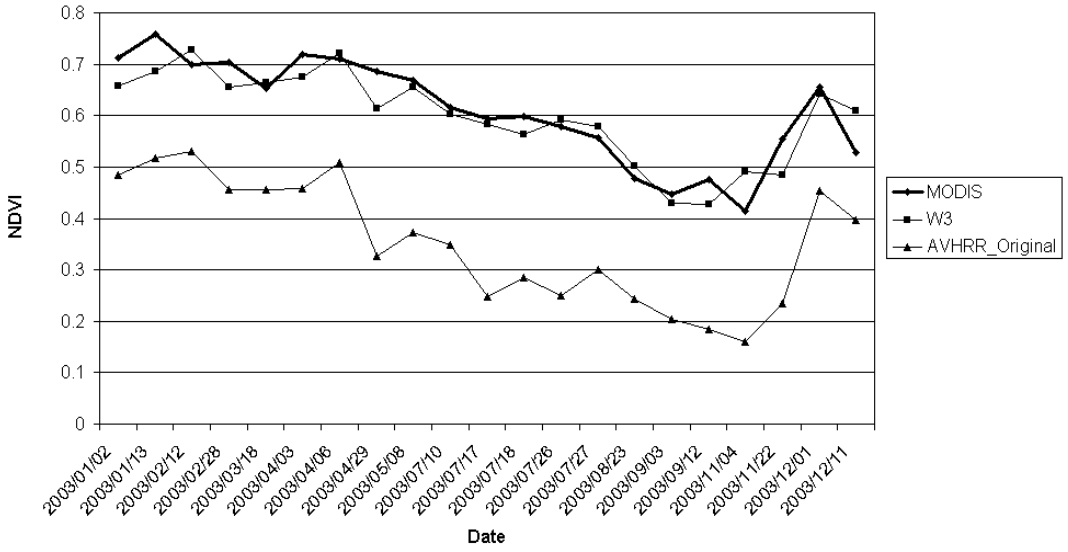

Fgure 4.22 Time-series of NDVI data for uncorrected and corrected AVHRR data and for MODIS data for a point situated in a Bushland land-cover class.

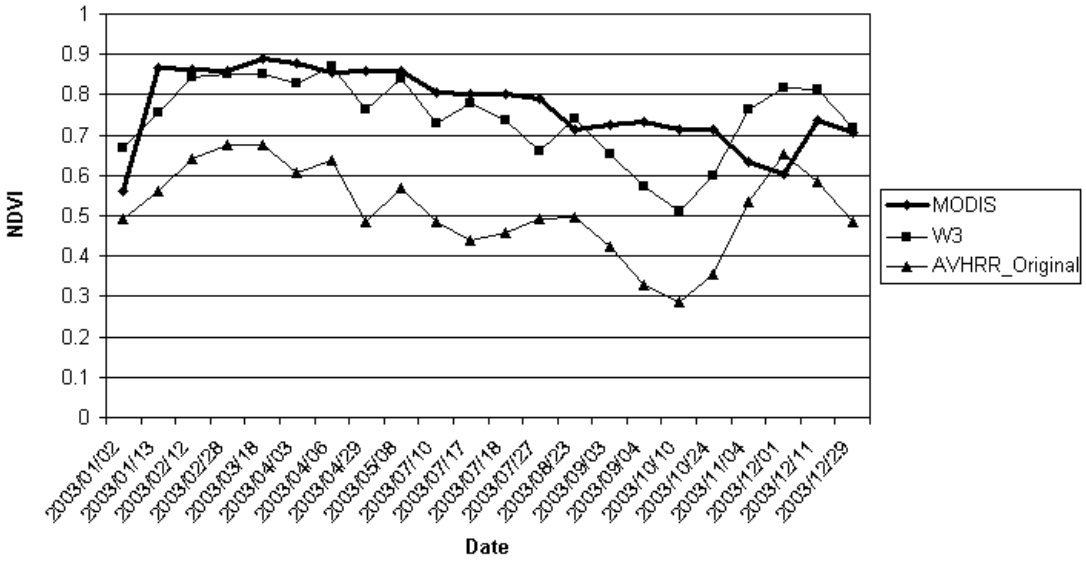

Figure 4.23 Time-series of NDVI data for uncorrected and corrected AVHRR data and for MODIS data for a point situated in a Natural Forest land-cover class.

The MODIS NDVI and the MODIS-equivalent NDVI through application of methods W2 and W3 to AVHRR data for daily data during 2003 are indicated in figure 4.24.

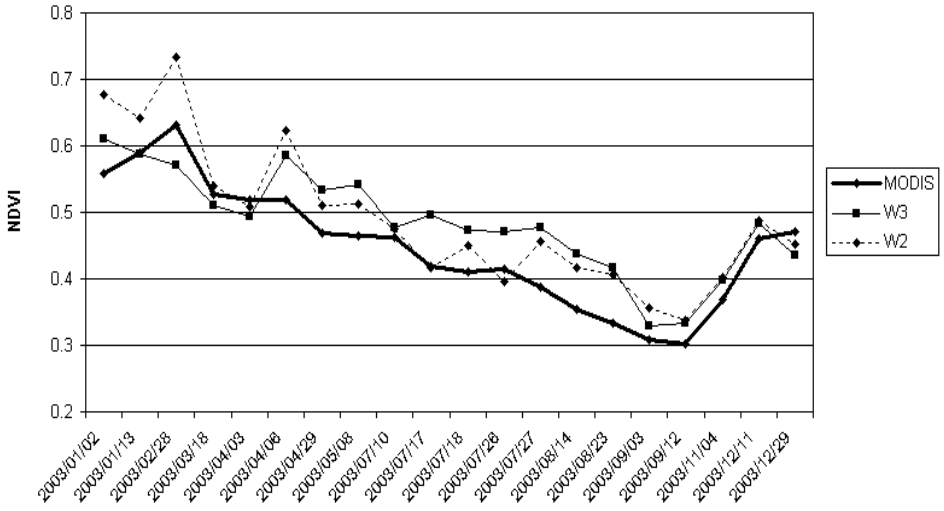

Figure 4.24 Time-series of NDVI data for uncorrected and corrected AVHRR data and for MODIS data for a point situated in a Subsistance-Dryland land-cover class

The three methods (W1, W2 and W3) to estimate a MODIS-equivalent NDVI from AVHRR data were compared. Figure 4.25 indicates the root-mean-square error made when estimating a MODIS-equivalent NDVI for all the points and all 26 days by all three methods. These root-mean-square errors vary between half and two standard deviations of the MODIS 16-daycomposite NDVI values as calculated from the data for the year 2002 (figure 4.26). When the root-mean-square error is considered, each method from W1 to W3 respectively slightly outperformed the previous one.

The importance of atmospheric correction becomes slightly clearer when the data are classed according to the total precipitable water content of the atmosphere (Figure 4.27). The root-mean-square error of the methods for when the atmospheric precipitable water content is lower than 3 g cm^{-2} and when it is higher than 3 g.cm^{-2} is portrayed. From the 375 instances comprising the daily data, 87 were for days when the precipitable water content of the atmosphere exceeded 3 g cm^{-2}. In the 6S code, 3 g cm^{-2} is used for the default precipitable water content of a tropical atmosphere.

It must be taken into account that only cloudless days and days with very little cloud cover were considered for extraction of data for daily values, hence minimizing the occurrence of high precipitable water amounts in the data. On the other hand, multi-day composites made of the historical NDVI will also compensate for atmospheric effects by selecting the days with relatively less atmospheric contamination.

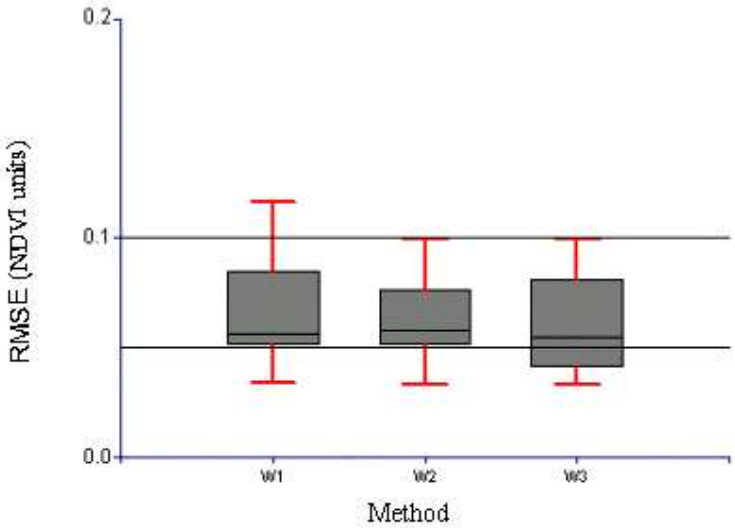

Figure 4.25 Box plot indicating the characteristics of the root-mean-square error when using different methods to estimate a MODIS-equivalent NDVI from daily AVHRR data during 2003.

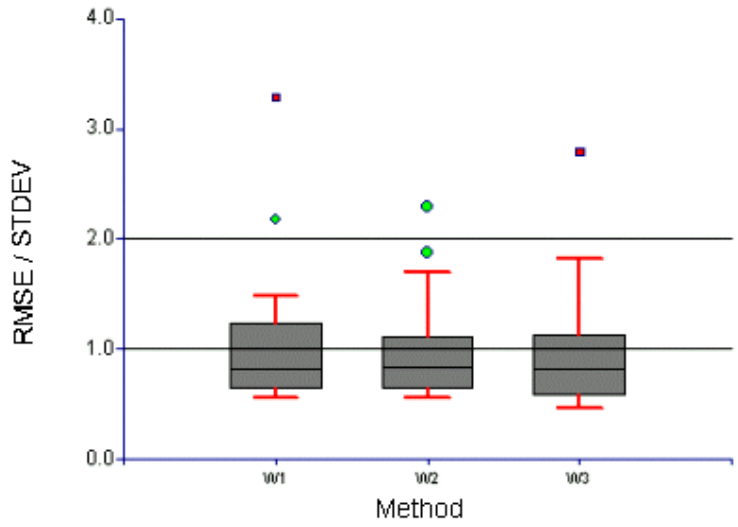

Figure 4.26 Box plot of root-mean-square errors of MODIS-equivalent NDVI estimation from daily AVHRR data during 2003, expressed as multiple of the standard of MODIS composite NDVI values deviation at each point throughout 2002.

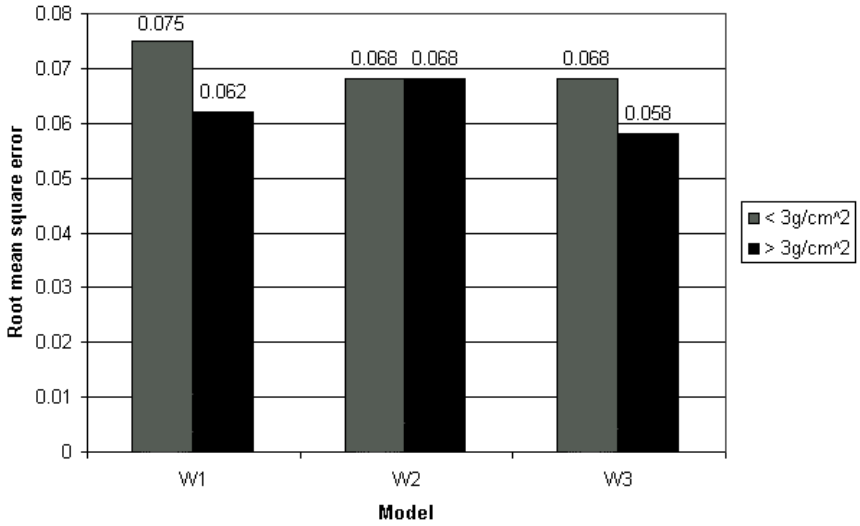

Figure 4.27 Root-mean-square errors of the models at different total precipitable water contents of the atmosphere.

To formulate an idea of the significance of any improvement resulting from atmospheric correction to the AVHRR data, the paired-wise Student's t-test was performed on the absolute errors that resulted from estimating MODIS-equivalent daily NDVI values as by means of method W2 and W3. With a P (T<=t) value of 0.24, no significant difference was

indicated between the accuracy of the respective methods. The results from the t-test are indicated in Table 4.2.

Table 4.2 Result of paired t-test performed on methods W2 and W3

Mean (W2)	0.0531
Variance (W2)	0.0018
Mean (W3)	0.0506
Variance (W3)	0.0017
Observations	375
Pearson Correlation	0.4892
Hypothesized Mean Difference	0
Degrees of freedom	374
t Stat	1.1727
P(T<=t) two-tail	0.2416
t Critical two-tail	2.5891

4.3 Effect of miss-registration of AVHRR data

The geo-location procedure applied during the processing of AVHRR data produces images that are correct to within two pixels. For the composites made, visual inspection and manual adjustments were used to keep the registration within one pixel. Cloudless images over the area of interest from the archive covering a 45-day period were inspected. The geo-locations for three of the images were out by two pixels (Table 4.3).

Table 4.3 Miss-registration of AVHRR pixels over a 45-day period.

	Miss-registration			
Total Images	0 pixel	1 pixels	1.5 pixels	2 pixels
15	4	5	3	3

The image-to-image registration of the MODIS data was more stable and a shift in excess of half a pixel was not observed.

For different errors in geo-location of images, the resultant decline in regression correlation was investigated. The R-squared value between two images for all the points

when various shifts in the relative position of one image to the other were considered differed with respect to direction of pixel-shift.

Between the two identical AVHRR images, the R-squared value decreased by only 0.02 to 0.05 with a one-pixel shift, but with a shift of 2 pixels it decreased by between 0.07 and 0.43. The R-squared values between AVHRR and MODIS fell in a similar fashion and it can be seen that the decline in R-Squared values are much larger beyond 1 pixel shift than between no shift and one pixel shift. The contribution of miss-registration of the AVHRR data within a pixel on the decrease in the R-squared value is less than 0.07, but for a two-pixel shift it dropped by about 0.45 (Figure 4.28 and figure 4.29).

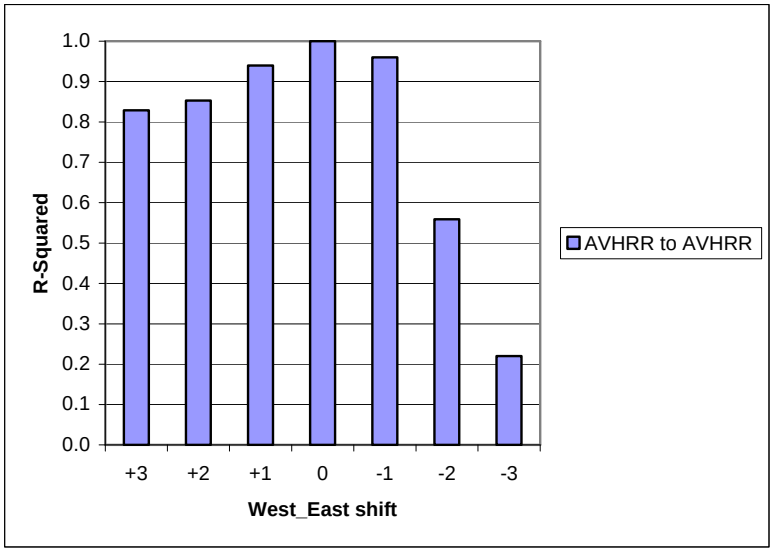

Figure 4.28 Miss-registration and coupled decline in R-Squared values.

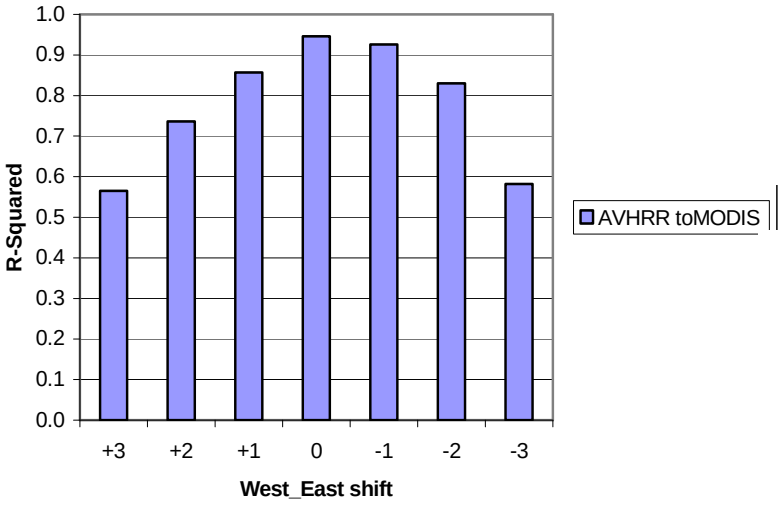

Figure 4.29 Miss-registration and coupled decline in R-squared values.

The difference between the NDVI values of the same AVHRR image for all the points could be seen to increase in magnitude and variability with increased miss-registration (Figure 4.30). For a two-pixel miss-registration, the magnitude of change in the NDVI value for the points, within the inter-quartile range, could be as high as 0.06, which is the same as the standard deviation for most of the sites (Figure 4.5) and also of the same magnitude as the errors made by applying the three methods of estimating a MODIS-equivalent NDVI from AVHRR NDVI values. For a shift of three pixels, as is possible on days with extensive cloud cover, the error is even larger and outside the range of the errors made when estimating the MODIS-equivalent NDVI from the AVHRR NDVI.

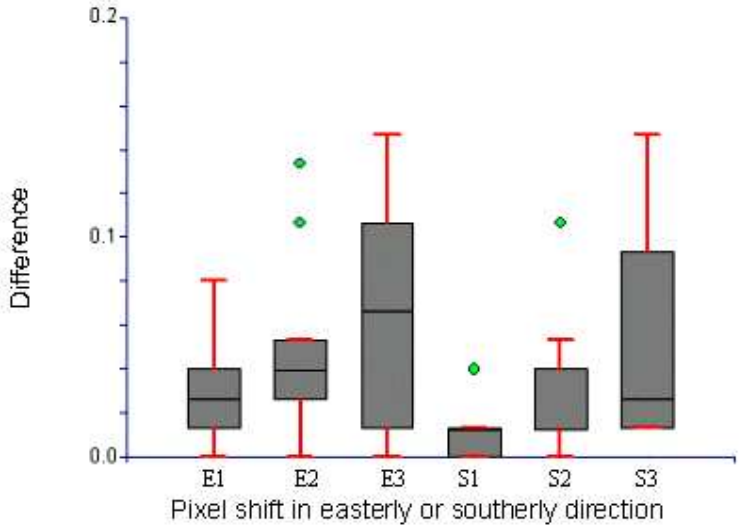

Figure 4.30 Miss-registration in an easterly and southerly direction respectively and coupled increase in absolute difference between two AVHRR NDVI images of the same day.

It can be seen that because of the north-south orientation of the coastline, the north-south alignment of mountain ranges and the resultant north-south orientation of land-cover classes in the area an east-west shift created larger differences and can lead to larger errors than north-south shift.

5. CONCLUSIONS AND RECOMMENDATIONS

A strong linear relationship was found between the mean AVHRR- and mean MODIS NDVI. The mean value referred to is the seasonally averaged NDVI as derived from NDVI composite data. However, between specific points, significant variation in the relationship was detected. This variation was partially compensated for by incorporating the mean AVHRR NDVI value into the relationship. This resulted in a location-specific method that relates the slope and intercept of the linear relation between MODIS NDVI values and AVHRR NDVI values to the mean AVHRR value. This method slightly outperformed the use of a singular constant linear relationship for all the areas. The performance of the method was more consistent over the whole range of NDVI values and is therefore applicable over a wider range of land-cover types, because the mean AVHRR and MODIS NDVI were shown to be land-cover related.

The preferred method can estimate a MODIS-equivalent NDVI with a root-mean-square error that ranges between 0.03 and 0.1 NDVI units. The mean root-mean-square error resulting from using the method to estimate a MODIS-equivalent NDVI from the AVHRR NDVI is 0.05 NDVI units. Out of 17 points, the method estimated the MODIS-equivalent NDVI to within one standard deviation of the MODIS NDVI for 11 of the points. Only for one point, the root-mean-square error exceeded two standard deviations of the MODIS NDVI determined over an entire year.

Even if the preferred method is not the method of choice for implementation at the ISCW, it still highlights the fact that there is a land-cover related influence on the relation between the AVHRR and MODIS NDVI. The reason why the mean AVHRR NDVI was proposed as a surrogate for land-cover class differences was that land-cover is fragmented and variation occurs on scales smaller than what is represented by AVHRR pixels. Furthermore, using the mean AVHRR NDVI image in the correction procedure will not result in spatial inconsistencies as the use of land-cover type-specific models could.

Atmospheric correction through the 6S code only slightly improved on the method, specifically when precipitable water amounts were high. The increase in accuracy when atmospheric correction was applied to the data as opposed to when no atmospheric

correction was applied was not statistically significant. Furthermore, the atmospheric data used was of a finer spatial resolution than what is available historically. Uncertainties introduced by historical atmospheric data include the coarse spatial resolution and the fact that for most variables, only total column density data is available, not profile data. The computationally exhaustive nature of implementing atmospheric correction is another factor discouraging the use of radiative transfer models throughout a long dataset. The creation of composites through the CA-MVC method already compensates for some of the atmospheric influences. In the light of the abovementioned facts, atmospheric correction is not recommended for the historical dataset.

Compensating for the BRDF was not implemented on either of the datasets (MODIS or AVHRR). Analysis was constrained to within a 45° view angle for both sensors in order to compensate for some of the effects of BRDF. Corrections for BRDF in the 6S code are land-cover specific and not recommended for inhomogeneous areas, as is frequently covered by an AVHRR pixel.

The geo-location accuracy of the automatic processing procedures at the ISCW needs to be improved. Currently accuracy to within two AVHRR pixels is achieved when cloud cover is low. However, if cloud cover is substantial during image acquisition, the geo-location can be out by three pixels. Over the area of interest, this could double or even triple the error when estimating a MODIS-equivalent NDVI from AVHRR NDVI imagery.

Based on the results reported, the following recommendations are made regarding a method to estimate a MODIS-equivalent NDVI from AVHRR data:

- The historical AVHRR dataset needs to be assessed in terms of inter-calibration of the various AVHRR sensors in use during the development of the historical dataset. Updated versions of post-launch calibration parameters for the two visible channels (Tahnk and Coakley, 2001; Heidinger *et al.*, 2003, Rao and Chen 1995, 1996) should be implemented.
- The geo-location precision of the automatic image processing procedures at the ISCW should be improved to one pixel. Manual intervention as one of the final processing steps in the geo-location procedure is recommended.
- All composites of NDVI data should be made within an angle of 45°.

Following these preliminary steps, the rest of the procedure is indicated in figure 5.1.

The length of a historical compositng period is not dictated by this procedure. However, if atmospheric correction is not applied, a compositing period of 16 days instead of 10 days is recommended in order to increase the effectiveness in terms of compensating for the effects of the atmosphere. The mean AVHRR NDVI image can be updated at intervals during the period of the historical AVHRR NDVI record to update the slope and intercept of the relationship between the AVHRR and MODIS NDVI for use with earlier imagery.

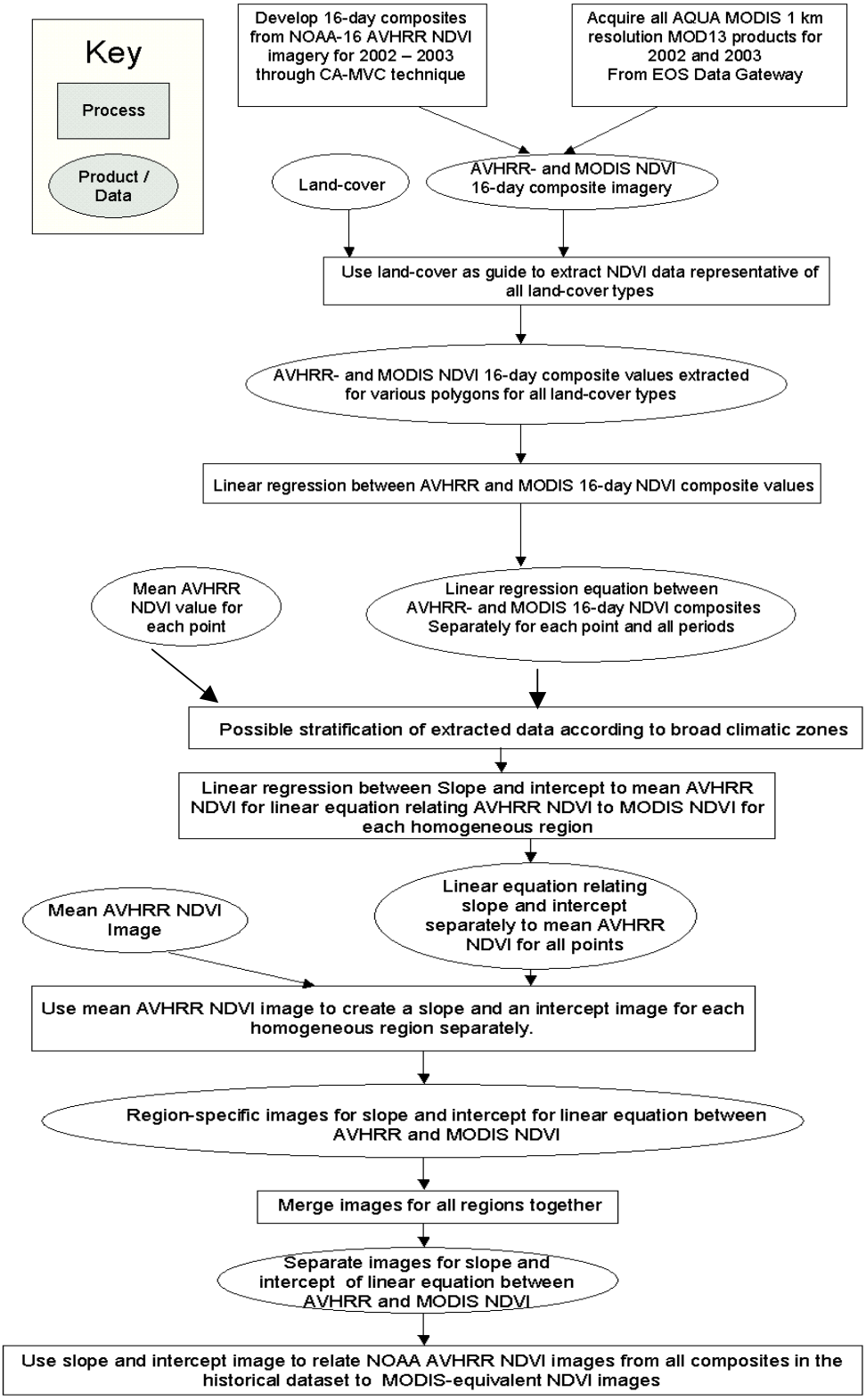

Figure 5.1 Flowchart indicating processes and data involved in the proposed method to estimate a MODIS–equivalent NDVI from the AVHRR NDVI.

REFERENCES

Agbu P. A. and James M. E. (1994) *The NOAA/NASA Pathfinder AVHRR land dataset user's manual.* Goddard Distributed Active Archive Centre, NASA Goddard Space Flight Centre, Greenbelt, MD, USA.

Awaya Y., Kodani E., Tanaka K., Liu J., Zhuang D. and Meng Y. (2004) Estimation of global net primary productivity using NOAA images and meteorological data changes between 1988 and 1993. *International Journal of Remote Sensing*, **25**, 1597 – 1613.

Celestrak (2005) Website www.celestrak.com

Chi H. (2003) Partial atmospheric correction of NOAA AVHRR data using the bare-sand soil line method. *International Journal of Remote Sensing*, **24**, 3369 – 3379.

Chopping M.J. (2001) Testing LiSK models over a semi-arid grassland region with visible and near-infrared ATSR-2 and AVHRR data. *International Journal of Remote Sensing*, **22**, 3533 – 3552.

Cihlar J., Manak D. and Voisin, N. (1994) AVHRR bidirectional reflectance effects and compositing. *Remote Sensing of Environment*, **48**, 77 – 88.

Coetz S. J. (1997) Multi-sensor analysis of NDVI, surface temperature and biophysical variables at a mixed grassland site. *International Journal of Remote Sensing*, **18**, 71 − 94.

Cracknell A.P. (1997) *The Advanced Very High Resolution Radiometer*. Taylor and Francis, Dundee.

Dabrowska-Zielinska, K., Kogan F., Ciolkosz A., Grusszcynska M. and Kowalik W. (2002) Modelling of crop yield and crop growth conditions in Poland using AVHRR-based indices. *International Journal of Remote sensing*, **23**, 1109 – 1123.

Didan K. and Huete A. (2002) MODIS Vegetation Index collection 4 readiness website. Website http://landdb1.nascom.nasa.gov/production/Collection4/Readiness_Meeting_121702/MOD13_C004_Readiness.pdf.

EOS Data Gateway (2005) Website http://edcimswww.cr.usgs.gov/pub/imswelcome/

Fairbanks D. H. K., Thompson M. W., Vink D. E., Newby T. S., Van den Berg H. M. and Everard D. A. (2000) The South African land-cover characteristics database: a synopsis of the landscape. *South African Journal of Science*, **96**, 69 – 82.

Fensholt R. (2004) Earth observation of vegetation status over the Sahelian and Sudanian West Africa: Comparison of TERRA MODIS and NOAA AVHRR satellite data. *International Journal of Remote Sensing*, **25**, 1641 – 1659.

GACP (2005) Global Aerosol Climatology Project. Website http://gacp.giss.nasa.gov/

Gallo K. P. and Daughtry C. S. T. (1987) Differences in vegetation indices for simulated Landsat-5 MSS and TM, NOAA-9 AVHRR and SPOT-1 sensor systems. *Remote Sensing of Environment*, **23**, 439 – 452.

Gao X., Huete A. R., Ni W. and Miura T. (2000) Optical – biophysical relationships of vegetation spectra without background contamination. *Remote Sensing of Environment*, **74**, 609 – 620.

Gitelson A. A. and Kaufman Y. J. (1998) MODIS NDVI optimization to fit the AVHRR data series – spectral considerations. *Remote Sensing of Environment*, **66**, 343 – 350.

Gitelson A. and Merzylak M. (1996) Signature analysis of leaf reflectance spectra: Algorithm development for remote sensing of Chlorophyll. *Journal of Plant Physiology*, **148**, 494 – 500.

Goward, S. N., Markham B., Dye D. G., Dulaney W. and Yang J. (1991) Normalized difference vegetation index measurements from the Advanced Very High Resolution Radiometer. *Remote Sensing of Environment*, **35**, 257 – 277.

Goward S. N. and Huemerich, K. F. (1992) Vegetation canopy PAR absorptance and the normalized difference vegetation index: an assessment using the SAIL method. *Remote Sensing of Environment*, **39**, 119 – 140.

Guenther B., Xiong X., Salomonson V. V., Barnes W. L. and Young J. (2002) On-orbit performance of the Earth Observing System Moderate Resolution Imaging Spectroradiometer, first year of data. *Remote Sensing of Environment*, **83,** 16 – 30.

Gutman G. G. (1999) On the use of long-term global land reflectances and vetgetation indices derived from the Advanced Very High Resolution Radiometer. *Journal of Geophysicla Research*, **104**, 6241 – 6255.

Hanan N. P., Prince S. P. and Holben B. N. (1995) Atmospheric correction of AVHRR data for biophysical remote sensing of the Sahel. *Remote Sensing of Environment*, **51**, 306 – 316

Hansen L. (1999) Chips for Windows Version 4.5 – User's Guide, Copenhagen.

Hatfield J. L., Kanemasu E. T., Arsar G., Jackson R. D., Pinter P. J. jr., Reginato R. J. and Idso S. B. (1985) Leaf-area estimates from spectral measurements over various planting dates of wheat. *International Journal of Remote Sensing*, **6**, 167 – 175.

Heidinger A. K., Sullivan J. T. and Nagaraja Rao C. R. (2003) Calibration of visible and near-infrared channels of the NOAA-12 AVHRR using time series of observations over deserts. *International Journal of Remote Sensing*, **24**, 3635 – 3649.

Henschel J., Pauw J., Banyikwa F., Brito R., Chabwela H., Palmer T., Ringrose S., Santos L., Sito A. and Van Jaarsveld A. (2003) Developing the Environmental Long-Term Observatories Network of South Africa (ELTOSA). *South African Journal of Science*, **99,** 100 – 108.

Holben B. N. and Fraser R. S. (1984) Red and near-infrared sensor response to off-nadir viewing. *International Journal of Remote Sensing*, **5**, 160 – 170.

Holben B. N. (1986) characteristics of maximum-value composite images from temporal AVHRR data. *International Journal of Remote Sensing*, **7**, 1417 – 1434.

Hu B., Lucht W., Strahler A. H., Schaaf C. B. and Smith M. (2000) Surface albedos and angle-corrected NDVI from AVHRR observations of South America. *Remote Sensing of Environment*, **71**, 119 – 132.

Huete A. R. (1988) A Soil-adjusted vegetation index (SAVI). *Remote Sensing of Environment*, **25**, 295 – 309.

Huete A., Didan K., Miura T., Rodriguez E. P., Gao X. and Ferreira L. G. (2002) Overview of the radiometric and biophysical performance of the MODIS vegetation indices. *Remote Sensing of Environment*, **83,** 195 – 213.

Huete A., Justice C. and Liu H. (1994) Development of vegetation and soil indices for MODIS-EOS. *Remote Sensing of Environment*, **49**, 224 – 234.

Huete A. and Justice C. (1996) MODIS vegetation index (mod13) algorithm theoretical basis document. Version 2. Website http://modland.nascom.nasa.gov.

ISRDS/1 (2000) The Integrated Sustainable Rural Strategy – Strategy Document, Office of the President, Government of South Africa, Pretoria.

ISCCP (2005) International Satellite Cloud Climatology Project. Website http://isccp.giss.nasa.gov/docs/response.html#noa

Jiang D., Yang X., Clinton, N. and Wang N. (2004) An artificial neural network model for estimating crop yields using remotely sensed information. *International Journal of Remote Sensing*, **9**, 1723 – 1732.

Jupp D. L. B. (2000) A compendium of Kernel and other (semi-) empirical BRDF models. Website http://www.cossa.csiro.au/tasks/brdf/k_summ.pdf (Accessed - 2005)

Justice C. O., Eck T. F., Tanre D. and Holben B. N. (1991) The effect of water vapor on the normalized difference vegetation index derived for the Sahelian region from NOAA AVHRR data. *International Journal of Remote Sensing*, **12**, 1165 – 1187

Justice C. O., Salomonson V. V., Privette J., Riggs G., Strahler A., Lucht W., Myneni R., Knjazihhin Y., Running S., Nemani R., Vermote E., Townsend J. R. G., Defries R., Roy D., Wan Z., Huete A., van Leeuwen R., Giglio L., Muller J., Muller P., Lewis P. and Barnsley M (1998) The Moderate Resolution Imaging Spectroradiometer (MODIS): land remote sensing for global change research. *IEEE Transactions in Geoscience and Remote Sensing*, **36**, 1228 – 1249.

Justice C. O., Townshend J. R. G., Vermote E. F., Masuoka, E., Wolfe R. E., Saleous, N. and Roy D. P. and Morisette J. T. (2002) An overview of the MODIS Land data processing and product status. *Remote Sensing of Environment*, **83**, 3 – 15

Kalubarme M. H., Ptdar M. B., Manjunath K. R., Mahey R. K. and Siddhu S. S. (2003) Growth profile based crop yield models: a case study of large area wheat yield modeling and its extendibility using atmospheric corrected NOAA AVHRR data. *International Journal of Remote Sensing*, **24**, 2037 – 2054.

Kaufman Y. J. and Sendra C. (1988) Algorithm for Automatic atmospheric correction to visible and near infrared satellite imagery. *International Journal of Remote Sensing*, **9**, 1357 – 1381.

King M. D., Platnick S., Moeller C. C., Revercomb H. E. and Chu D. A. (2002) Remote sensing of smoke, land and clouds with the NASA ER-2 during SAFARI 2000. *Journal of Geophysical Research*, DOI 10.1029/2002JD002313.

LDAAC (2004) Land Distributed Active Archive Center. Website http://edcdaac.usgs.gov/tools/modis/.

LDOPE (2004) Land Data Operational Product Evaluation. Website http://landdb.nascom.nasa.gov/cgi-bin/QA_WWW.

Li Z., Cihlar J., Zheng X., Moreau L. and Ly H. (1996) The bidirectional effects of AVHRR data over Boreal regions. *IEEE Transactions on Geoscience and Remote Sensing*, **34**, 1308 – 1322.

Lillesand T.M. and Kiefer R.W. (2000) *Remote Sensing of the Environment*, fourth edition. John Wiley, New York.

LTER (2005) Long-Term Ecological Research. Website http://www.ilternet.edu/

Maselli F., Romanelli S., Bottai L. and Maracchi G. (2000) Processing of GAC NDVI data for yield forecasting in the Sahelian region. *International Journal of Remote Sensing*, **21**, 3509 – 3523.

MODIS web (2005) MODIS Data Summary. Website http://modis.gsfc.nasa.gov/data/summary.html

MODLAND Browse (2005) MODIS Land Products Browse Website. Website http://landqa2.nascom.nasa.gov/browse/browse.cgi

Moody A. and Strahler A. H. (1994) Characteristics of composited AVHRR data and problems in their classification. *International Journal of Remote Sensing*, **15**, 3473 – 3491.

Morisette J. T., Privette J. L. and Justice C. O. (2002) A framework for the validation of MODIS Land products. *Remote Sensing of Environment*, **83,** 77 – 96.

MYD07 Product Description (2005) Website http://modis-atmos.gsfc.nasa.gov/MOD07_L2/

MYD04 Product Description (2005) Website http://modis-atmos.gsfc.nasa.gov/MOD04_L2/

NASA (2004) National Aeronautics and Space Administration. Website http://earth.nasa.gov/

NCEP Reanalysis (2005) National Center for Environmental Prediction Reanalysis Data website. http://www.cdc.noaa.gov/cdc/data.ncep.reanalysis.html

Rao C. N. R. and Chen J. (1995) Inter-satellite calibration linkages for the visible and near-infrared channels of the Advanced Very High Resolution Radiometer on NOAA-1, -9 and –11 spacecraft. *International Journal of Remote Sensing*, **16**, 1931 – 1942.

Rao C. N. R. and Chen J. (1996) Post-launch calibration of the visible and near-infrared channels of the Advanced Very High Resolution Radiometer on the NOAA-14 spacecraft. *International Journal of Remote Sensing*, **17**, 2743 – 2747.

Reynolds C. A., Yitayew M., Slack D. C., Hutchinson C. F., Huete A. and Peterson M. S. (2000) Estimating crop yields and production by integrating the FAO Crop Specific Water Balance model with real-time satellite data and ground-based ancillary data. *International Journal of Remote Sensing*, **21**, 3487 – 3508.

Roujean J. L., Leroy M. and Deschamps P. Y. (1992) A bidirectional reflectance model of the Earth's surface for the correction of remote sensing data. *Journal of Geophysical Research*, **97**, 20 455 – 20 486.

Rahman H. and Diedieu G. (1994) SMAC: A simplified method for the atmospheric correction of satellite measurements in the solar spectrum. *International Journal of Remote Sensing*, **15**, 123 – 143.

SAEON (2005) South African Ecological Observatory Network. Website http://www.nrf.ac.za/saeon/documents.html

Salama M. S. and Monbaliu J. (2004) Atmospheric correction of Advanced Very High Resolution imagery. *International Journal of Remote Sensing*, **25**, 1349 – 1355.

Simpson J. J. and Stitt J. R. (1998) A procedure for the detection and removal of cloud cover from AVHRR data over land. *IEEE Transactions on Geoscience and Remote Sensing*, **36**, 880 – 897.

Steven M. D., Malthus T. J., Baret F. and Xu H. (2003) Inter-calibration of vegetation indices from different sensor systems. *Remote sensing of Environment*, **88**, 412 – 422.

Strohmenger P. H. E., Van der Merwe J. P. A., Smith H. M., Van den Berg H. M., Van den Berg E. C., Malherbe J., De Nysschen G., Van der Waldt M., Haasbroek P., Morgenthal T., Kelltner K. and Van Rensburg L.(2004) Auditing the status of the Natural Resources in the OR Tambo and Umkhanyakude ISRDS nodes. ARC – ISCW Report No. GW/A/2003/47/1, Institute for Soil Climate and Water, Pretoria.

Swap R. J., Annegarn H. J., Otter, L. (2002) Southern African regional Science Initiative (SAFARI 200): summary of science plan. *South African Journal of Science*, **98,** 107 – 208.

Tahnk W. R. and Coakley J. A. (2001) Improved calibration coefficients for NOAA-14 visible and near-infrared channels. *International Journal of Remote Sensing*, **22**, 1269 – 1283.

TERRA (2004) Website http://terra.nasa.gov/

TERRA Readiness Document (2004) Website landweb.nascom.nasa.gov/prod_www/Collection**4**/ TERRA/Readiness_Meeting_121702/MOD13_C00**4**_Readiness.pdf

TOMS (2005) Total Ozone Spectrometer Fact Page. Website http://toms.gsfc.nasa.gov/index.html

Townshend J. R. G. and Justice C. O. (2002) Towards operational monitoring of terrestrial systems by moderate-resolution remote sensing. *Remote Sensing of Environment*, **83,** 351 – 359.

Trischenko A. P., Cihlar J. and Li Z. (2002) Effects of spectral response function on surface reflectance and NDVI measured with moderate resolution satellite sensors. *Remote Sensing of Environment*, **88**, 1 – 18.

Tucker C. J., Vanpreat C. L., Sharman M. J. and Van Ittersum G. (1985) Satellite remote sensing of total herbaceous biomass production in the Senegalese Sahel: 1980 – 1984. *Remote Sensing of Environment*, **17**, 233 – 249.

Vermote E. F., Tanre D., Dueze J. L., Herman M. and Morcrette J. J. (1997a) Second simulation of the satellite signal in the solar spectrum, 6S: an overview. *IEEE Transactions on Geoscience and Remote Sensing*, **35**, 675 – 686.

Vermote E. F., El Saleous N., Justice C. O., Kaufman Y. J., Privette J. L., Remer L., Roger J. C. and Tanre D. (1997b) Atmospheric correction of visible to middle infra-red EOS-MODIS data over land surface: Background, operational algorithm and validation. *Journal of Geophysical Research*, **102**, 17 131 – 17 141.

Vermote E. F., Tanre D., Dueze J. L., Herman M. and Morcrette J. J. (1997c) 6S User Guide Version 2, July 1997.

Vermote E. F. and Vermeulen A. (1999) MODIS Algorithm technical background document: Atmospheric correction algorithm: Spectral reflectances (MOD09), Version 4. Department of Geography, University of Maryland, Greenbelt MD.

Wessels K. J., Prince S. D., Frost P. E. and van Zyl D. (2004) Assessing the effects of human-induced land degradation in the former homelands of South Africa with 1 km AVHRR NDVI time-series. *Remote Sensing of Environment*, **91**, 47 – 67.

Wolfe R. E., Nishihama M., Fleig A. J., Kuyper J. A., Roy D. P., Storey J. C. and Pratt F. S (2002) Achieving sub-pixel geolocation accuracy in support of MODIS land science. *Remote Sensing of Environment*, **83,** 31 – 49.

Wu A., Li X. and Cihlar, J. (1995) Effects of BRDF and cover type and greenness on Advanced Very High resolution Radiometer reflectances: analysis and removal. *Journal of Geophysical Research*, **100**, 9179 – 9192.

Zhao W., Tamura M. and Takahashi H. (2000) Atmospheric and spectral corrections for estimating surface albedo from satellite data using 6S code. *Remote Sensing of Environment*, **76**, 202 – 212.

APPENDIX I

Table A 1 MODIS bands and their applications

Band #	Pixel Resolution (m)	Reflected Bandwidth Range (nm)	Emitted Bandwidth Range (µm)	Potential Applications
1	250	620-670		Absolute Land Cover Transformation, Vegetation Chlorophyll
2	250	841-876		Cloud Amount, Vegetation Land Cover Transformation
3	500	459-479		Soil/Vegetation Differences
4	500	545-565		Green Vegetation
5	500	1230-1250		Leaf/Canopy Differences
6	500	1628-1652		Snow/Cloud Differences
7	500	2105-2155		Cloud Properties, Land Properties
8	1000	405-420		Chlorophyll
9	1000	438-448		Chlorophyll
10	1000	483-493		Chlorophyll
11	1000	526-536		Chlorophyll
12	1000	546-556		Sediments
13h	1000	662-672		Atmosphere, Sediments
13l	1000	662-672		Atmosphere, Sediments
14h	1000	673-683		Chlorophyll Fluorescence
14l	1000	673-683		Chlorophyll Fluorescence
15	1000	743-753		Aerosol Properties
16	1000	862-877		Aerosol Properties, Atmospheric Properties
17	1000	890-920		Atmospheric Properties, Cloud Properties
18	1000	931-941		Atmospheric Properties, Cloud Properties
19	1000	915-965		Atmospheric Properties, Cloud Properties
20	1000		3.660-3.840	Sea Surface Temperature
21	1000		3.929-3.989	Forest Fires and Volcanoes
22	1000		3.929-3.989	Cloud Temperature, Surface Temperature
23	1000		4.020-4.080	Cloud Temperature, Surface Temperature
24	1000		4.433-4.498	Cloud Fraction, Troposphere Temperature

Band #	Pixel Resolution (m)	Reflected Bandwidth Range (nm)	Emitted Bandwidth Range (µm)	Potential Applications
25	1000		4.482-4.549	Cloud Fraction, Troposphere Temperature
26	1000	1360-1390		Cloud Fraction (Thin Cirrus), Troposphere Temperature
27	1000		6.535-6.895	Mid Troposphere Humidity
28	1000		7.175-7.475	Upper Troposphere Humidity
29	1000		8.400-8.700	Surface Temperature
30	1000		9.580-9.880	Total Ozone
31	1000		10.780-11.280	Cloud Temperature, Forest Fires and Volcanoes, Surface Temp.
32	1000		11.770-12.270	Cloud Height, Forest Fires and Volcanoes, Surface Temperature
33	1000		13.185-13.485	Cloud Fraction, Cloud Height
34	1000		13.485-13.785	Cloud Fraction, Cloud Height
35	1000		13.785-14.085	Cloud Fraction, Cloud Height
36	1000		14.085-14.385	Cloud Fraction, Cloud Height

(Data source: http://synergy1.csr.utexas.edu/DataUsersGuide/MODISbands.html)

Table A 2 Quality assurance data description.

Bit No.	Parameter Name	Bit Comb.	Description
0-1	VI Quality (MODLAND Mandatory QA Bits)	00	VI produced with good quality
		01	VI produced but with unreliable quality and thus examination of other QA bits recommended
		10	VI produced but contaminated with clouds
		11	VI not produced due to bad quality
2-5	VI Usefulness Index	0000	Perfect quality (equal to VI quality = 00: VI produced with good quality)
		0001	High quality
		0010	Good quality
		0011	Acceptable quality
		0100	Fair quality
		0101	Intermediate quality
		0110	Below intermediate quality
		0111	Average quality
		1000	Below average quality

		1001	Questionable quality
		1010	Above marginal quality
		1011	Marginal quality
		1100	Low quality
		1101	No atmospheric correction performed
		1110	Quality too low to be useful
		1111	Not useful for other reasons (equal to VI quality = 11: VI not produced due to bad quality)
6-7	Aerosol Quantity	00	Climatology used for atmospheric correction
		01	Low
		10	Intermediate
		11	High
8	Atmosphere Adjacency Correction	0	(No) No adjacency correction performed
		1	(Yes) Adjacency correction performed
9	Atmosphere BRDF Correction	0	(No) No atmosphere-surface BRDF coupled correction performed
		1	(Yes) Atmosphere-surface BRDF coupled correction performed
10	Mixed Clouds	0	(No) No mixed clouds
		1	(Yes) Possible existence of mixed clouds
11-12	Land/Water Mask	00	Ocean/inland water · Shallow ocean · Moderate and continental ocean · Deep ocean · Deep inland water
		01	Coastal region · Ocean coastlines and lake shorelines · Shallow inland water
		10	Wetland · Ephemeral water
		11	Land
13	Snow/Ice	0	(No) No snow/ice
		1	(Yes) Possible existence of snow/ice
14	Shadow	0	(No) No shadow
		1	(Yes) Possible existence of shadow
15	Compositing Method	0	BRDF composite method used for compositing
		1	Constraint view angle MVC (CV-MVC) method used for compositing

(Data Source: MODIS User Guide, 20004. http://tbrs.arizona.edu/project/MODIS/)